MACROSCOPIC FLUID MODELS WITH LOCALIZED KINETIC UPSCALING EFFECTS*

PIERRE DEGOND†, JIAN-GUO LIU‡, AND LUC MIEUSSENS†

Abstract. This paper presents a general methodology to design macroscopic fluid models that take into account localized kinetic upscaling effects. The fluid models are solved in the whole domain together with a localized kinetic upscaling that corrects the fluid model wherever it is necessary. This upscaling is obtained by solving a kinetic equation on the nonequilibrium part of the distribution function. This equation is solved only locally and is related to the fluid equation through a downscaling effect. The method does not need to find an interface condition as do usual domain decomposition methods to match fluid and kinetic representations. We show our approach applies to problems that have a hydrodynamic time scale as well as to problems with diffusion time scale. Simple numerical schemes are proposed to discretize our models, and several numerical examples are used to validate the method.

Key words. kinetic-fluid coupling, kinetic equation, hydrodynamic approximation, diffusion approximation

AMS subject classifications. 82B40, 82B80, 82C40, 82C80, 76P05

DOI. 10.1137/060651574

1. Introduction.

The simulation of particle systems is a typical example of multiscale problems. Indeed, an accurate description of such systems is given by the kinetic theory. But when the system is close to an equilibrium state, it is much simpler and often accurate enough to use macroscopic models like fluid mechanics or diffusion theory. A rough indicator of the validity of a macroscopic approximation is often called the Knudsen number, which can be defined as the ratio of the mean free path of the particles to a typical macroscopic length. Among the very large spectrum of problems of particle systems, we simply mention the classical rarefied gas dynamics, neutron transport, and radiative transfer. Recently new fields have been investigated as granular media or traffic theory.

Until a recent period, macroscopic approximations (that we call "fluid" in this article) were used even for systems far from equilibrium, since microscopic theories were too computationally expensive. Nowadays, modern supercomputers are able to treat many problems at the kinetic level, but there are still very challenging problems, like those involving different scales. For instance, we mention the simulation of reentry problems in aerodynamics, where the particles are close to equilibrium far from the reentry body, while nonequilibrium effects are very large close to the body. For radiative transfer problems, this can occur when the material is composed of several parts of very different opacities. The difficulty is that the computational effort is generally increasing with the inverse of the Knudsen number. Then a large part of the computational time is due to a part of the system (close to equilibrium) that could be more efficiently described by a simpler macroscopic model.

*Received by the editors February 6, 2006; accepted for publication (in revised form) July 5, 2006; published electronically November 14, 2006.

http://www.siam.org/journals/mms/5-3/65157.html

†MIP, UMR 5640 (CNRS-UPS-INSA), Université Paul Sabatier, 118, Route de Narbonne, 31062 Toulouse cedex, France (degond@mip.ups-tlse.fr, mieussens@mip.ups-tlse.fr).

‡Institute for Physical Science and Technology and Department of Mathematics, University of Maryland, College Park, MD 20742-4015 (jliu@math.umd.edu). This author's research was partially supported by NSF grant DMS 05-12176.

Consequently, it seems very natural to try to solve each model wherever it is appropriate, the main problem being to correctly match the two descriptions at the interfaces of the different domains. This is especially attractive when the particles are in an equilibrium state in the major part of the domain. This idea has been largely explored in the past few years. For problems involving diffusive fluid models (like for neutron and radiative transfer problems) we mention, for instance, the works of Bal and Maday [2], Degond and Schmeiser [16], Golse, Jin, and Levermore [19], Klar [23], and Klar and Siedow [26]. For rarefied gas dynamics, we mention the works of Bourgat, Le Tallec, and Tidriri [5], Qiu [35], Le Tallec and Mallinger [37], Klar, Neunzert, and Struckmeier [24], Schneider [36], and Chen et al. [9]. The main common feature of these approaches is that they are typical domain decomposition techniques where the fluid and kinetic models are solved in different subdomains. The coupling relations are defined through suitable boundary conditions at the interface between the subdomains. More recently, different approaches using a local kinetic description of the particles according to some physical criterion were proposed by Tiwari [38] and Ohsawa and Ohwada [32]. We also mention the hybrid methods of Crouseilles, Degond, and Lemou [11, 12] in which a domain decomposition technique is used in velocity space.

The domain decomposition strategy has also been widely used in molecular dynamics problems. The computational domain is decomposed into two atomistic and continuum regions on which the atomistic and continuum models are used, respectively, and some matching condition is devised for the continuum-atomistic interface (see, for instance, Cai et al. [6], E and Huang [18], Abraham et al. [1], Wagner, Karpov, and Liu [39], Li and E [28], and E and Engquist [17]). However, these molecular dynamics problems are quite different from kinetic models. In particular, the equilibrium state is not well defined.

Very recently, a different approach has been proposed by Degond and Jin [14] for matching kinetic and diffusion problems. In this work the idea was still to use a domain decomposition method but in which the coupling is through the equations rather than the boundary conditions. This is done by using a buffer zone around the interface, and an artificial transition function that smoothly passes from 1 in the kinetic domain to 0 in the diffusion zone. The solution of the original transport equation is recovered as the sum of the solutions of the two models. This is different from the usual domain decomposition methods in which each of the models represents the full solution. The transition function makes the equation on each domain degenerate at the end of the buffer zone; thus no boundary condition is needed at this interface. This idea results in a very easy-to-use method that works very well in the linear case. This has been successfully extended by Degond, Jin, and Mieussens [15] to nonlinear kinetic models that have hydrodynamic fluid approximations. However, an important property has been noted in [15]: namely, the equilibrium distribution must be a homogeneous function of the macroscopic quantities to ensure that uniform flows are preserved by the matching model. This property is satisfied for the important problems of rarefied gas dynamics but not for particles as in nonlinear radiative transfer problems. It has been shown in [15] that this nonpreservation of uniform flows generates oscillations in the results.

While we use several ideas from the previous methods, our idea is rather different. We solve the fluid model in the whole domain together with a localized kinetic upscaling that corrects the fluid model wherever it is necessary. The perturbative kinetic equation is solved only locally and is related to the macroscopic equation through a downscaling effect. Indeed, we separate the distribution function into an equilibrium leading part (that can be described by the macroscopic fluid variables) plus a pertur-

bative nonequilibrium distribution. This perturbative part is localized by using the idea of buffer zones and transition functions as proposed in [14] and [15]. We point out that here the transition function is applied to the perturbative nonequilibrium part of the distribution.

We show that a robust matching can be achieved by putting the buffer zone in the fluid zone and using asymptotic preserving schemes. We obtain a method that shares many advantages of the method of [14] and [15]: namely, it is easy to use and to implement, and it is computationally economic.

In addition, this new method turns to be very general, since it does not require any homogeneity property of the equilibrium distribution, as opposed to the method of [14] and [15]. It can be applied to very different physical problems, and in particular, we show that it works fairly well for the nonlinear radiative heat transfer problem that was not tractable with the previous method.

We also point out other differences with the method proposed in [15]. Essentially the method in [15] is a domain decomposition approach, since the fluid and the kinetic models are defined in almost different domains. Namely, the fluid density is zero in the kinetic zone. Even with the Boltzmann equation for which [15] applies quite well, this can lead to serious numerical problems, since this produces an artificial cavitation phenomenon. This is difficult to solve with classical numerical techniques, such as particle methods or hyperbolic schemes that are not very efficient in case of vacuum (Roe scheme for instance). On the contrary in our work, the method we propose is based on a fluid model defined everywhere in which the density is never artificially set to zero. It is only locally corrected by a kinetic upscaling, which seems physically more natural. At the numerical level, these new models are slightly more complicated than the models of [15], but we show with several tests that in practice this does not really give any difficulties. One can also wonder whether our method is not computationally more expensive than in [15], in particular for the kinetic zones where we solve a kinetic equation and a moment system instead of a single kinetic equation. But in practice, since the computational cost for solving the kinetic equation is far larger than the one of the moment system—by several orders of magnitude—then the total cost of our method is comparable to [15].

We now give the outline of the article. In section 2, we present a very general kinetic model, with a few important properties, and its associated decomposition into microscopic upscaling and macroscopic downscaling. Most of the usual kinetic models can be written in this form. We show that the microscopic upscaling can be split by using a buffer zone and a transition function. From this model we deduce in section 3 a macroscopic fluid model with localized kinetic upscaling effects, and we study some of its properties. Two simple examples of applications are also given. We apply the same strategy for the diffusion scaling in section 4, with again two different examples. The numerical methods are given in section 5. In section 6, we present several numerical tests to illustrate the potential of our approach. Finally, a short conclusion is given in section 7.

2. Basic strategy.

2.1. Kinetic model. We present the method on a general kinetic equation in one space dimension. Let $f(t,x,v)$ represent the density of particles that at time t have position $x \in (0,1)$ and velocity $v \in \mathbb{R}$ or any bounded or discrete subset of $\mathbb{R}$. The kinetic equation is

$$\partial_t f + v\partial_x f = Q(f), \tag{2.1}$$

with initial data

$$f|_{t=0} = f_{init}.$$

The left-hand side of (2.1) describes the motion of the particles along the x-axis with velocity v, while the operator Q takes into account the collisions between particles. This operator acts on f only through the velocity locally at each (t, x).

The integral of any scalar or vector valued function $f = f(v)$ over the velocity set is denoted by $\langle f \rangle = \int f(v)\, dv$.

The collision operator Q is assumed to satisfy the local conservation property

$$\langle mQ(f) \rangle = 0 \qquad \text{for every } f,$$

where $m(v) = (m_i(v))_{i=1}^d$ are locally conserved quantities. Consequently, multiplying (2.1) by m and integrating over the velocity set gives the local conservation laws

$$\partial_t \langle mf \rangle + \partial_x \langle vmf \rangle = 0. \tag{2.2}$$

Finally, we assume that the local equilibria of Q (i.e., the solutions of $Q(f) = 0$) are equilibrium distributions $E[\rho]$, uniquely specified by their moments ρ through the relation

$$\rho = \langle mE[\rho] \rangle. \tag{2.3}$$

We do not specify boundary conditions for the moment.

2.2. Asymptotic fluid models: Hydrodynamic versus diffusion scalings. When the mean free path of the particles is very small compared with the size of the domain, i.e., when Q is "large," the numerical resolution of (2.1) can be very expensive, and it is worth using the asymptotic model obtained when Q "tends to infinity." Then an adapted scaling of the time and space variables must be chosen. Indeed, we have to use a new set of macroscopic variables x' and t' according to

$$x' = \varepsilon x, \quad t' = \varepsilon t \qquad \text{(hydrodynamic scaling)},$$

or

$$x' = \varepsilon x, \quad t' = \varepsilon^2 t \qquad \text{(diffusion scaling)}.$$

This choice is mainly guided by the structure of the collision operator. Roughly speaking, if the flux vector $\int vE[\rho]$ of particles in the associated equilibrium state is zero, then this means that the macroscopic flow is slow, and that a large macroscopic time scale must be chosen, hence the diffusion scaling. On the contrary, if this flux is nonzero, then the hydrodynamic scaling gives the correct result.

Although these ideas will be explained in detail in sections 3 and 4, we briefly review the two kinds of fluid models that can be obtained with these two scalings.

Typically, when the hydrodynamic scaling is adapted to the structure of the kinetic model, one obtains a hyperbolic fluid model for ρ of type

$$\partial_t \rho + \partial_x F(\rho) = 0.$$

When the diffusion scaling has to be used, one obtains a parabolic fluid model for ρ, that is to say a diffusion equation, of type

$$\partial_t \rho - \partial_x (D \partial_x \Phi(\rho)) = 0.$$

2.3. Microscopic upscaling and macroscopic downscaling. The micro-macro decomposition of f consists in separating f into two equilibrium and non-equilibrium parts. We define the function g such that

$$f = E[\rho] + g, \tag{2.4}$$

where $\rho := \langle mf \rangle$ are the d first moments of f. This means that g represents the nonequilibrium part of the distribution f. First, note that since the equilibrium has the same moments as f (see (2.3)), then the corresponding moments of g are zero:

$$\langle mg \rangle = 0. \tag{2.5}$$

Consequently, we can easily derive the formal result.

PROPOSITION 2.1. *If $\rho = \langle mf \rangle$ and $g = f - E[\rho]$, then they satisfy the following coupled equations:*

$$\partial_t \rho + \partial_x F(\rho) + \partial_x \langle vmg \rangle = 0, \tag{2.6}$$

$$\partial_t g + v\partial_x g = Q(E[\rho] + g) - (\partial_t + v\partial_x)E[\rho], \tag{2.7}$$

where $F(\rho) = \langle vmE[\rho] \rangle$ is the equilibrium flux vector. The associated initial data are

$$\rho|_{t=0} = \rho_{init} = \langle mf_{init} \rangle \quad \text{and} \quad g|_{t=0} = f_{init} - E[\rho_{init}].$$

Reciprocally, if ρ and g satisfy this system, then $f = E[\rho] + g$ satisfies the kinetic equation (2.1)*, and we have $\rho = \langle mf \rangle$ and $\langle mg \rangle = 0$.*

The upscaling term in (2.6) is $\partial_x \langle vmg \rangle$, while the downscaling term in (2.7) is $-(\partial_t + v\partial_x)E[\rho]$.

Proof. First, we inject relation (2.4) into the local conservation laws (2.2) to find

$$\partial_t \left(\langle mE[\rho] \rangle + \langle mg \rangle \right) + \partial_x \left(\langle vmE[\rho] \rangle + \langle vmg \rangle \right) = 0.$$

Then we use the definition of the equilibrium flux vector $F(\rho)$ given in the proposition and relation (2.3) and (2.5) to find (2.6). Relation (2.7) is directly derived from (2.4) and (2.1).

Reciprocally, assume that ρ and g satisfy system (2.6)–(2.7). Then if we set $f = E[\rho] + g$, it is clear from (2.7) that f satisfies (2.1). Moreover, taking the moments of (2.7) and using (2.6) gives $\partial_t \langle mg \rangle = 0$. Since these moments are zero at $t = 0$ due to the initial data, then $\langle mg \rangle = 0$ anytime, and hence $\langle mf \rangle = \langle mE[\rho] \rangle = \rho$. ∎

Note that this decomposition is very classical. For instance, it is often used to derive Navier–Stokes equations from the Boltzmann equation in rarefied gas dynamics by the Chapman–Enskog procedure (see [7]). We take the name "micro-macro" decomposition from the paper by Liu and Yu [29].

Remark 2.1. This decomposition considerably simplifies (2.1) if Q is a relaxation operator towards $E[\rho]$, as, for instance, with the BGK operator of rarefied gas dynamics [3] $Q(f) = \nu(E[\rho] - f)$. In that case, the collision term in the right-hand side of (2.7) is nothing but $-\nu g$, that is, a linear term.

Remark 2.2. It is well known that the time derivative $\partial_t E[\rho]$ can be eliminated in (2.7) (see the classical Chapman–Enskog expansion in [7]). But we do not find this technique very convenient for numerical reasons: this makes some nonconservative products appear in the equations that are difficult to approximate numerically.

2.4. Splitting of the perturbative nonequilibrium effects by using a transition function. Now we apply the strategy of [14] and [15] to the nonequilibrium part g of model (2.6)–(2.7).

As a simple example, we define a buffer interval $[a, b]$. We introduce a smooth function $h(x)$ such that

$$\begin{cases} h(x) = 1 & \text{for} \quad x \le a, \\ h(x) = 0 & \text{for} \quad x \ge b, \\ h(x) \in [0,1] & \text{for} \quad a \le x \le b. \end{cases}$$

If we define the two distributions $g_K = hg$ and $g_F = (1-h)g$, then it is easy to check that they satisfy the following coupled system:

$$\partial_t \rho + \partial_x F(\rho) + \partial_x \langle v m g_K \rangle + \partial_x \langle v m g_F \rangle = 0, \tag{2.8}$$

$$\partial_t g_K + hv\partial_x g_K + hv\partial_x g_F = hQ(E[\rho] + g_K + g_F) - h(\partial_t + v\partial_x)E[\rho], \tag{2.9}$$

$$\begin{aligned} &\partial_t g_F + (1-h)v\partial_x g_F + (1-h)v\partial_x g_K \\ &\qquad = (1-h)Q(E[\rho] + g_K + g_F) - (1-h)(\partial_t + v\partial_x)E[\rho], \end{aligned} \tag{2.10}$$

with initial data

$$\rho|_{t=0} = \rho_{init}, \quad g_K|_{t=0} = h(f_{init} - E[\rho_{init}]), \quad g_F|_{t=0} = (1-h)(f_{init} - E[\rho_{init}]). \tag{2.11}$$

Indeed, we note the following.

PROPOSITION 2.2. *If (ρ, g_K, g_F) is the solution of problem (2.8)–(2.10) with initial data (2.11), then $(\rho, g = g_K + g_F)$ is the solution of problem (2.6)–(2.7) with initial condition $(\rho_{init}, f_{init} - E[\rho_{init}])$. Moreover, the moments of g_K and g_F are zero: $\langle m g_K \rangle = \langle m g_F \rangle = 0$.*

Reciprocally, if (ρ, g) is the solution of (2.6)–(2.7), then $(\rho, g_K, g_F) = (\rho, hg, (1-h)g)$ is the solution of (2.8)–(2.10) with the same initial condition.

Proof. Just add (2.9) and (2.10). For the converse statement, note that

$$\begin{aligned} \partial_t g_K = h\partial_t g &= -hv\partial_x g + hQ(E[\rho] + g) - h(\partial_t + v\partial_x)E[\rho] \\ &= -hv\partial_x(g_K + g_F) + hQ(E[\rho] + g_K + g_F) - h(\partial_t + v\partial_x)E[\rho], \end{aligned}$$

which gives (2.9). Equation (2.10) is also obtained in this way. ∎

Note that due to their definition, $g_K(t, ., .) = 0$ for $t \ge 0$ and $x \ge b$, and reciprocally $g_F(t, ., .) = 0$ for $t \ge 0$ and $x \le a$.

Now the idea is to note that if the flow is close to equilibrium in the right part $x \ge b$, then the asymptotic procedure mentioned in section 2.2 can be used in this zone to obtain a coupled model between ρ and g_K only. This is what we explain in detail for both the hydrodynamic and the diffusion scalings in the following sections.

3. Localization of the perturbative nonequilibrium effects: The hydrodynamic scaling. First, we detail how one can pass from the kinetic equation (2.1) to a hydrodynamic model. With the hydrodynamic scaling $x' = \varepsilon x$, $t' = \varepsilon t$, (2.1) reads

$$\partial_t f^\varepsilon + v\partial_x f^\varepsilon = \frac{1}{\varepsilon} Q(f^\varepsilon). \tag{3.1}$$

Therefore, if we assume that f^ε goes to $f^{(0)}$ as ε tends to 0, then passing to the limit in (3.1) gives $Q(f^0)$, and hence $f^{(0)}$ is an equilibrium distribution $E[\rho^{(0)}]$. Since the conservation laws are

$$\partial_t \rho^\varepsilon + \partial_x \langle v m f^\varepsilon \rangle = 0,$$

we can also pass to the limit in these relations to obtain

$$\partial_t \rho^{(0)} + \partial_x F(\rho^{(0)}) = 0 \tag{3.2}$$

with the equilibrium flux vector $F(\rho^{(0)}) = \langle v m E[\rho^{(0)}] \rangle$. This is the asymptotic hydrodynamic model for (3.1).

Now we explain how the same procedure can be done with the system (2.8)–(2.10) if the flow is close to the equilibrium in one part of the domain only. The scaled system (2.8)–(2.10) reads

$$\partial_t \rho^\varepsilon + \partial_x F(\rho^\varepsilon) + \partial_x \langle v m g_K^\varepsilon \rangle + \partial_x \langle v m g_F^\varepsilon \rangle = 0, \tag{3.3}$$

$$\partial_t g_K^\varepsilon + h v \partial_x g_K^\varepsilon + h v \partial_x g_F^\varepsilon = \frac{1}{\varepsilon} h Q(E[\rho^\varepsilon] + g_K^\varepsilon + g_F^\varepsilon) - h(\partial_t + v\partial_x) E[\rho^\varepsilon], \tag{3.4}$$

$$\begin{aligned} &\partial_t g_F^\varepsilon + (1-h) v \partial_x g_F^\varepsilon + (1-h) v \partial_x g_K^\varepsilon \\ &\qquad = \frac{1}{\varepsilon}(1-h) Q(E[\rho^\varepsilon] + g_K^\varepsilon + g_F^\varepsilon) - (1-h)(\partial_t + v\partial_x) E[\rho^\varepsilon]. \end{aligned} \tag{3.5}$$

Assume that Q is of order ε in the interval $(-\infty, a)$ and of order 1 in $(a, +\infty)$. In other words, we consider that the left region must be treated by a kinetic model, while the right region can be approximated by the hydrodynamic equations. Therefore, we shall be allowed only to perform the hydrodynamic approximation on (3.5), while (3.4) will have to stay untouched. To this end, the collision term of (3.5) is rewritten as $Q(E[\rho^\varepsilon] + g_K^\varepsilon + g_F^\varepsilon) = Q(E[\rho^\varepsilon] + g_F^\varepsilon) + [Q(E[\rho^\varepsilon] + g_K^\varepsilon + g_F^\varepsilon) - Q(E[\rho^\varepsilon] + g_F^\varepsilon)]$, and we assume that $Q(E[\rho^\varepsilon] + g_F^\varepsilon)$ is $O(1)$, whereas $[Q(E[\rho^\varepsilon] + g_K^\varepsilon + g_F^\varepsilon) - Q(E[\rho^\varepsilon] + g_F^\varepsilon)]$ is an $O(\varepsilon)$. Then (3.5) is rewritten as follows:

$$\begin{aligned} &\varepsilon \partial_t g_F^\varepsilon + \varepsilon(1-h) v \partial_x g_F^\varepsilon - (1-h) Q(E[\rho^\varepsilon] + g_F^\varepsilon) \\ &\qquad = -\varepsilon(1-h) v \partial_x g_K^\varepsilon - \varepsilon(1-h)(\partial_t + v\partial_x) E[\rho^\varepsilon] \\ &\qquad\quad + (1-h)[Q(E[\rho^\varepsilon] + g_K^\varepsilon + g_F^\varepsilon) - Q(E[\rho^\varepsilon] + g_F^\varepsilon)], \end{aligned} \tag{3.6}$$

where the right-hand side is considered to be $O(\varepsilon)$.

The following proposition states the limit $\varepsilon \to 0$ of g_F^ε.

PROPOSITION 3.1. *Consider* (3.6)*, where the right-hand side is treated as an* $O(\varepsilon)$ *term. Then as* $\varepsilon \to 0$, $g_F^\varepsilon \to 0$.

Proof. We first note that $\langle m g_F^\varepsilon \rangle = 0$ for every ε from Proposition 2.2. Consequently, this is also true in the limit $\varepsilon = 0$, that is,

$$\langle m g_F^{(0)} \rangle = 0. \tag{3.7}$$

Now we let ε go to 0 in (3.6) to find $Q(E[\rho^{(0)}] + g_F^{(0)}) = 0$, and hence $E[\rho^{(0)}] + g_F^{(0)} = E[\rho^*]$. Then using (3.7) and relation (2.3) gives $\rho^* = \rho^{(0)}$, and hence $g_F^{(0)} = 0$. ∎

Consequently, the last equation (3.5) of our system can be eliminated. Moreover, we can replace g_F^ε by 0 in the first two equations (3.3) and (3.4), and we obtain the

following coupled model:

$$\partial_t \rho^\varepsilon + \partial_x F(\rho^\varepsilon) + \partial_x \langle vm g_K^\varepsilon \rangle = 0, \tag{3.8}$$

$$\partial_t g_K^\varepsilon + hv\partial_x g_K^\varepsilon = \frac{h}{\varepsilon} Q(E[\rho^\varepsilon] + g_K^\varepsilon) - h(\partial_t + v\partial_x)E[\rho^\varepsilon], \tag{3.9}$$

with initial data

$$\rho|_{t=0} = \rho_{init}^\varepsilon, \quad g_K^\varepsilon|_{t=0} = h(f_{init} - E[\rho_{init}]).$$

Therefore this coupled model will be used to approximate by $E[\rho^\varepsilon] + g_K^\varepsilon$, the solution f^ε of model (3.1). More precisely, f^ε is supposed to be approximated by $E[\rho^\varepsilon] + g_K^\varepsilon$ in $(-\infty, a)$ and (a, b), and by $E[\rho^\varepsilon]$ in $(b, +\infty)$. Remark that in the kinetic zone (where $h = 1$), the coupled model gives the original equation in its micro-macro decomposition form (2.6)–(2.7). In the fluid zone (where $h = 0$) $g_K = 0$ and (3.8) gives the hydrodynamic model (3.2). The transition function plays only a role in the buffer zone where $0 < h < 1$.

Note that this system is very similar to the microscopic upscaling/macroscopic downscaling system (2.6)–(2.7). However, both upscaling and downscaling terms now are localized. We thus call this system a macroscopic fluid model with localized kinetic upscalings. It will be shortly named "micro-Macro fluid model" in the remaining sections.

In the following sections, we give some interesting properties of this model, and we give two simple examples of application.

To simplify the notation in the remainder of the paper, the superscript ε will be omitted when no confusion is caused.

3.1. Properties of the micro-Macro model.

3.1.1. Preservation of uniform flows. Uniform flows for model (2.1) are constant equilibrium distributions $f = E[\rho]$. Because of the function h, f is approximated in the micro-Macro model (3.8)–(3.9) by nonuniform distributions $E[\rho] + g_K$. Then it is not clear whether this approximation is still a uniform distribution. However, this preservation property is desirable to prevent oscillations in zones where the flow should be uniform (a similar phenomenon is known in computational fluid dynamics when one wants to discretize conservation laws written in curvilinear coordinates; see [40]). As it is shown in the following proposition, the preservation of uniform flows is well satisfied by our model.

PROPOSITION 3.2. *If the initial condition f_{init} is a constant equilibrium $E[\rho_{init}]$, then $\rho = \rho_{init}$ and $g_K = h(f_{init} - E[\rho_{init}]) = 0$ are solutions of the micro-Macro model* (3.8)–(3.9)*, and $E[\rho] + g_K = E[\rho_{init}]$; that is, the kinetic/fluid solution of the micro-Macro model is exactly the solution of the original kinetic model.*

Proof. We put $\rho = \rho_{init}$ and $g_K = 0$ in the left- and right-hand sides of (3.8) and (3.9) and easily observe that these equations are satisfied. ∎

Remark 3.1. We recall that in the previous method of [15], this property was true only in the particular case where the equilibrium distribution is a homogeneous function of degree one with respect to its moments. As a consequence, the coupled model of [15] is not designed for particles governed by Fermi–Dirac or Bose–Einstein statistics, while it works well with Maxwell–Boltzmann statistics. This restriction does not occur here, since the transition function h operates only on the nonequilibrium part of the distribution. This will be clearly illustrated with the examples of sections 3.4 and 4.2.

3.1.2. Full hydrodynamic limit. Here we prove that if both regions are hydrodynamic, we recover the global hydrodynamic equation (3.2) for ρ.

PROPOSITION 3.3. *As $\varepsilon \to 0$, the moments ρ^ε of the micro-Macro model* (3.8)–(3.9) *converge to $\rho^{(0)}$, a solution of the hydrodynamic equation*

$$\partial_t \rho^{(0)} + \partial_x F(\rho^{(0)}) = 0, \tag{3.10}$$

with initial data

$$\rho^{(0)}|_{t=0} = \rho_{init}.$$

Proof. The proof is similar to what we did to derive the micro-Macro model. We first note that we can prove in the same manner as we did in the proof of Proposition 2.1 that $\langle m g_K^\varepsilon \rangle = 0$ for every ε. Consequently, this is also true at the limit $\varepsilon = 0$, that is,

$$\langle m g_K^{(0)} \rangle = 0. \tag{3.11}$$

Now we let ε go to 0 in (3.9) to find $Q(E[\rho^{(0)}] + g_K^{(0)}) = 0$, and hence $E[\rho^{(0)}] + g_K^{(0)} = E[\rho^*]$. Then using (3.11) gives $\rho^* = \rho^{(0)}$, and hence $g_K^{(0)} = 0$. Finally, we can pass to the limit in (3.8) to obtain the hydrodynamic equation (3.10). ∎

3.2. Correct placement of the buffer zone. Here we briefly describe how the derivation of the micro-Macro model (3.8)–(3.9) can be made more rigorously. In particular, our aim is to justify the assumption on the size of Q, and how ε can tend to zero in one zone and not in the other one.

If we consider a relaxation collision operator $Q(f) = (E[\rho] - f)$, like the BGK operator of rarefied gas dynamics, (2.9)–(2.10) simply read

$$\partial_t g_K + hv\partial_x g_K + hv\partial_x g_F = -\frac{1}{\tau} g_K - h(\partial_t + v\partial_x)E[\rho], \tag{3.12}$$

$$\partial_t g_F + (1-h)v\partial_x g_F + (1-h)v\partial_x g_K = -\frac{1}{\tau} g_F - (1-h)(\partial_t + v\partial_x)E[\rho], \tag{3.13}$$

where ε has been replaced by a function τ. Now we assume that τ is a nondecreasing function of x such that $\tau = \delta \ll 1$ in $(-\infty, b)$ and τ tends to 1 as x goes to $+\infty$. Then for every x, as $\delta \to 0$, $\tau(x)$ tends to a function τ_0 which is 0 in $(-\infty, b)$ and grows to 1 as x is large. Thus with (3.13) we see that g_F is an $O(\delta)$ in $(-\infty, b)$. Moreover, if the transition function h is defined as in section 2.4, then (3.13) gives $g_F = 0$ for $x \geq b$. Consequently, g_F globally tends to 0 as $\delta \to 0$, and we recover the micro-Macro model (3.8)–(3.9) with τ_0 instead of ε.

Note that in this derivation, we see the importance to place the buffer zone $[a, b]$ inside the fluid zone (that is, where τ is small). Indeed, it is fundamental that τ goes to zero inside the buffer zone to obtain that g_F is small everywhere.

3.3. Example 1: The BGK equation of rarefied gas dynamics. Here we apply our method to the BGK equation written in one dimension of space and one dimension of velocity

$$\partial_t f + v\partial_x f = Q(f) = \frac{1}{\varepsilon}(E[\rho] - f), \tag{3.14}$$

where $\rho = (n, nu, \frac{1}{2}nu^2 + \frac{1}{2}n\theta)$ and

$$E[\rho] = \frac{n}{(2\pi\theta)^{1/2}} \exp\left(-\frac{(v-u)^2}{2\theta}\right)$$

is the Maxwellian equilibrium distribution. This equation is clearly in the same form as (2.1) with $d = 3$ locally conserved quantities $m(v) = (1, v, \frac{1}{2}v^2)$.

As noted in Remark 2.1, this relaxation form of the collision operator considerably simplifies the micro-Macro model (3.8)–(3.9) that reads

$$\begin{aligned} &\partial_t \rho + \partial_x F(\rho) + \partial_x \langle v m g_K \rangle = 0, \\ &\partial_t g_K + hv\partial_x g_K = -\frac{1}{\varepsilon}\nu g_K - h(\partial_t + v\partial_x)E[\rho], \end{aligned} \tag{3.15}$$

where $F(\rho) = (nu, nu^2 + n\theta, u(\frac{1}{2}nu^2 + \frac{3}{2}n\theta))$. The corresponding full hydrodynamic model (3.10) in this case is the Euler equations of gas dynamics with $\gamma = 3$.

3.4. Example 2: The Jin–Xin relaxation model of the Burgers equation. This model (introduced in [22]) can be obtained from the following discrete-velocity kinetic model where the particles can have only velocities $+1$ and -1. It reads in the hydrodynamic scaling

$$\partial_t f_1 + \partial_x f_1 = \frac{1}{\varepsilon}(M_1[\rho] - f_1), \qquad \partial_t f_2 - \partial_x f_2 = \frac{1}{\varepsilon}(M_2[\rho] - f_2). \tag{3.16}$$

The collision operator is a relaxation operator towards the equilibrium

$$(M_1[\rho], M_2[\rho]) = \frac{1}{2}(\rho + F(\rho), \rho - F(\rho)),$$

where $\rho = f_1 + f_2$ is the only conserved quantity, and $F(\rho) = \frac{1}{2}\rho^2$. As explained in [15], this model cannot be correctly treated with the coupling developed in this reference, since the equilibrium is not a homogeneous function of ρ.

Defining $j = f_1 - f_2$, we can derive a system for ρ and j equivalent to (3.16)

$$\partial_t \rho + \partial_x j = 0, \qquad \partial_t j + \partial_x \rho = \frac{1}{\varepsilon}(F(\rho) - j), \tag{3.17}$$

which is the so-called Jin–Xin relaxation model of the Burgers equation. When ε goes to zero, it is clear that $j \to F(\rho)$ and then the first equation gives

$$\partial_t \rho + \partial_x F(\rho) = 0,$$

which is the inviscid Burgers equation.

Equation (3.16) has the same form as (2.1), and the micro-Macro model (3.8)–(3.9) reads in this case

$$\begin{aligned} &\partial_t \rho + \partial_x F(\rho) + \partial_x (g_K^1 - g_K^2) = 0, \\ &\partial_t \begin{pmatrix} g_K^1 \\ g_K^2 \end{pmatrix} + h\partial_x \begin{pmatrix} g_K^1 \\ -g_K^2 \end{pmatrix} = -\frac{1}{\varepsilon}\begin{pmatrix} g_K^1 \\ g_K^2 \end{pmatrix} - h\left(\partial_t \begin{pmatrix} M_1 \\ M_2 \end{pmatrix} + \partial_x \begin{pmatrix} M_1 \\ -M_2 \end{pmatrix}\right), \end{aligned} \tag{3.18}$$

which is very similar to the micro-Macro model (3.15) for the BGK model of section 3.3. However, it can be further simplified, since we can prove that the moment of (g_K^1, g_K^2) is zero (the proof is the same as in the proof of Proposition 2.2). Actually, this

means in this case that $g_K^2 = -g_K^1$. Then by defining the flux $J_K = g_K^1 - g_K^2 = 2g_K^1$ and substracting the two last equations of (3.18), we obtain the simplified micro-Macro model

$$\begin{aligned} &\partial_t \rho + \partial_x F(\rho) + \partial_x J_K = 0, \\ &\partial_t J_K = -\frac{1}{\varepsilon} J_K - h(\partial_t F(\rho) + \partial_x \rho). \end{aligned} \tag{3.19}$$

Note that the last equation is just a simple ordinary differential equation with a source term for J_K.

Finally, note that this system could directly be derived from the Jin–Xin form (3.17) of the discrete-velocity model (3.16) by applying the same strategy on the unknowns (ρ, j) instead of using (f_1, f_2). Namely, j is separated into $j = F(\rho) + J$ (this is the micro-macro decomposition), while ρ is untouched. Then J is written as $J = J_K + J_F$ with $J_K = hJ$ and $J_F = (1-h)J$. Finally, J_F is eliminated by passing to the limit $\varepsilon = 0$ in its evolution equation, and we find (3.19).

4. Localization of the perturbative nonequilibrium effects: The diffusion scaling. Contrary to the hydrodynamic scaling, it is difficult to treat the diffusion scaling in a very general case. Consequently, we prefer directly developing our strategy with two different examples. The first example treated in section 4.1 is linear, while the other one treated in section 4.2 is nonlinear.

4.1. An example from linear transport theory.

4.1.1. The linear transport equation and its diffusion limit. We consider the one group transport equation in slab geometry already used in [14]. This equation reads as (2.1), where

$$Q(f) = \sigma([f] - f),$$

with $[f] = \frac{1}{2}\int_{-1}^{1} f(v)\,dv$ the average value of f on the velocity set $V = [-1, 1]$. The collision operator has only one collision invariant $m(v) = 1$, and its equilibrium functions $E[\rho]$ are simply the distributions that do not depend on v, namely $E[\rho] = \frac{1}{2}\rho$.

In the diffusion scaling $x' = \varepsilon x$, $t' = \varepsilon^2 t$, (2.1) reads

$$\varepsilon^2 \partial_t f^\varepsilon + \varepsilon v \partial_x f^\varepsilon = Q(f^\varepsilon). \tag{4.1}$$

The diffusion approximation of this equation is classically obtained by using a Hilbert expansion of f^ε (see [14] for details or [8] for a complete classical reference). However, in view of developing our method, we find it more instructive to work on the nonequilibrium part $g^\varepsilon = f^\varepsilon - E[\rho^\varepsilon] = f^\varepsilon - \frac{1}{2}\rho^\varepsilon$ of the micro-macro decomposition (2.6)–(2.7) rewritten here with rescaled variables

$$\varepsilon \partial_t \rho^\varepsilon + \partial_x \langle v g^\varepsilon \rangle = 0, \tag{4.2}$$

$$\varepsilon^2 \partial_t g^\varepsilon + \varepsilon v \partial_x g^\varepsilon = -\sigma g^\varepsilon - \frac{1}{2}(\varepsilon^2 \partial_t + \varepsilon v \partial_x)\rho^\varepsilon, \tag{4.3}$$

with initial conditions

$$\rho^\varepsilon|_{t=0} = \rho_{init} = \langle f_{init} \rangle \quad \text{and} \quad g^\varepsilon|_{t=0} = f_{init} - \frac{1}{2}\rho_{init}.$$

We insert the Hilbert expansions

$$g^\varepsilon = g^{(0)} + \varepsilon g^{(1)} + O(\varepsilon^2) \quad \text{and} \quad \rho^\varepsilon = \rho^{(0)} + \varepsilon \rho^{(1)} + O(\varepsilon^2)$$

into (4.2)–(4.3) and identify the terms of equal power of ε. This leads to the sequence of equations

$$O(1) \text{ terms:} \qquad \partial_x \langle v g^{(0)} \rangle = 0 \quad \text{and} \quad g^{(0)} = 0,$$

$$O(\varepsilon) \text{ terms:} \qquad \partial_t \rho^{(0)} + \partial_x \langle v g^{(1)} \rangle = 0 \quad \text{and} \quad g^{(1)} = -\frac{1}{2\sigma} v \partial_x \rho^{(0)}.$$

These relations give the following diffusion equation satisfied by the limit $\rho^{(0)}$ of ρ^ε as ε goes to 0:

$$\partial_t \rho^{(0)} - \partial_x \left(\frac{1}{3\sigma} \partial_x \rho^{(0)} \right) = 0. \tag{4.4}$$

Note that due to the micro-macro decomposition, the Hilbert expansion procedure is slightly different from the usual one. For instance, we do not need the third order term of the development.

4.1.2. The micro-Macro model. For the rescaled linear transport model (4.1), the system (2.8)–(2.10) reads

$$\varepsilon \partial_t \rho^\varepsilon + \partial_x \langle v g_K^\varepsilon \rangle + \partial_x \langle v g_F^\varepsilon \rangle = 0, \tag{4.5}$$

$$\varepsilon^2 \partial_t g_K^\varepsilon + \varepsilon h v \partial_x g_K^\varepsilon + \varepsilon h v \partial_x g_F^\varepsilon = -\sigma g_K^\varepsilon - \tfrac{1}{2} h (\varepsilon^2 \partial_t + \varepsilon v \partial_x) \rho^\varepsilon, \tag{4.6}$$

$$\varepsilon^2 \partial_t g_F^\varepsilon + \varepsilon (1-h) v \partial_x g_F^\varepsilon + \varepsilon (1-h) v \partial_x g_K^\varepsilon = -\sigma g_F^\varepsilon - \tfrac{1}{2} (1-h) (\varepsilon^2 \partial_t + \varepsilon v \partial_x) \rho^\varepsilon, \tag{4.7}$$

with initial data

$$\rho^\varepsilon|_{t=0} = \rho_{init}, \quad g_K^\varepsilon|_{t=0} = h \left(f_{init} - \frac{1}{2} \rho_{init} \right), \quad g_F^\varepsilon|_{t=0} = (1-h) \left(f_{init} - \frac{1}{2} \rho_{init} \right).$$

Now we assume that σ is of order ε^2 in the interval $(-\infty, a)$, while it is of order 1 in $(a, +\infty)$. Therefore, we shall be allowed only to perform the diffusion approximation on g_F^ε, while g_K^ε will have to stay untouched. For this purpose, we rewrite (4.5) and (4.7) according to

$$\partial_x \langle v g_F^\varepsilon \rangle = -\varepsilon \partial_t \rho^\varepsilon - \partial_x \langle v g_K^\varepsilon \rangle, \tag{4.8}$$

$$\varepsilon^2 \partial_t g_F^\varepsilon + \varepsilon (1-h) v \partial_x g_F^\varepsilon + \sigma g_F^\varepsilon = -\varepsilon (1-h) v \partial_x g_K^\varepsilon - \tfrac{1}{2} (1-h) (\varepsilon^2 \partial_t + \varepsilon v \partial_x) \rho^\varepsilon, \tag{4.9}$$

where in the right-hand side of (4.8) and (4.9) the terms involving g_K^ε are assumed to be, respectively, of order ε and ε^2.

Following the procedure described in section 4.1.1, we insert the Hilbert expansions $g_F^\varepsilon = g_F^{(0)} + \varepsilon g_F^{(1)} + O(\varepsilon^2)$ and $\rho^\varepsilon = \rho^{(0)} + \varepsilon \rho^{(1)} + O(\varepsilon^2)$ into (4.8)–(4.9). We find the relations

$$O(1) \text{ terms:} \qquad \partial_x \langle v g_F^{(0)} \rangle = 0 \quad \text{and} \quad g_F^{(0)} = 0,$$

$$O(\varepsilon) \text{ terms:} \qquad \partial_x \langle v g_F^{(1)} \rangle = -\partial_t \rho^{(0)} - \partial_x \frac{1}{\varepsilon} \langle v g_K^\varepsilon \rangle \quad \text{and} \quad g_F^{(1)} = -\frac{1}{2\sigma} (1-h) v \partial_x \rho^{(0)}.$$

We note that the term involving g_K^ε is of order 1 by our hypothesis, despite its apparent dependence on ε. Using the last two relations, we find our micro-Macro model, which is the following diffusion equation for $\rho^{(0)}$ coupled with the kinetic equation (4.6):

$$\partial_t \rho^\varepsilon - \partial_x \left(\frac{1}{3\sigma} (1-h) \partial_x \rho^\varepsilon \right) + \partial_x \frac{1}{\varepsilon} \langle v g_K^\varepsilon \rangle = 0, \tag{4.10}$$

$$\varepsilon^2 \partial_t g_K^\varepsilon + \varepsilon h v \partial_x g_K^\varepsilon + \varepsilon h v \partial_x g_F^\varepsilon = -\sigma g_K^\varepsilon - \frac{1}{2} h (\varepsilon^2 \partial_t + \varepsilon v \partial_x) \rho^\varepsilon, \tag{4.11}$$

with

$$g_F^\varepsilon = -\varepsilon \frac{1}{2\sigma}(1-h) v \partial_x \rho^\varepsilon,$$

and with the initial data

$$\rho^\varepsilon|_{t=0} = \rho_{init}, \quad g_K^\varepsilon|_{t=0} = h\left(f_{init} - \frac{1}{2}\rho_{init}\right).$$

Note that $\rho^{(0)}$ is still denoted by ρ^ε in these relations, since it depends on ε through the coupling with g_K^ε.

Remark that in the kinetic zone (where $h = 1$), this micro-Macro model gives the original kinetic equation in its micro-macro decomposition form (4.2)–(4.3). In the fluid zone (where $h = 0$), (4.11) gives $g_K = 0$ and (4.10) gives the diffusion model (4.4). Thus our micro-Macro model is indeed a coupling between the original kinetic equation and its diffusion approximation.

As in section 3.2, this derivation can be made more rigorous by taking a particular σ and a well-located buffer zone (where σ is small).

4.1.3. Properties of the micro-Macro model. As for the micro-Macro model in the hydrodynamic scaling, we can easily prove the following properties.

PROPOSITION 4.1.

(i) *Preservation of uniform flows.*
If the initial condition f_{init} is a constant equilibrium $E[\rho_{init}] = \frac{1}{2}\rho_{init}$, then $\rho = \rho_{init}$ and $g_K = h(f_{init} - E[\rho_{init}]) = 0$ are solutions of the micro-Macro model (4.10)–(4.11)*, and $E[\rho] + g_K = E[\rho_{init}]$; that is, the solution of the micro-Macro model is exactly the solution of the original kinetic model.*

(ii) *Full diffusion limit.*
As ε goes to zero, the equilibrium part ρ^ε of the micro-Macro model converges to $\rho^{(0)}$, the solution of the diffusion equation (4.4)*.*

Proof. The proof of point (i) is very similar to that of Proposition 3.2 and is left to the reader.

For point (ii), we insert the Hilbert expansions $g_K^\varepsilon = g_K^{(0)} + \varepsilon g_K^{(1)} + O(\varepsilon^2)$ and $\rho^\varepsilon = \rho^{(0)} + \varepsilon\rho^{(1)} + O(\varepsilon^2)$ into (4.10)–(4.11) to obtain

$$O(1) \text{ terms:} \qquad \langle v g_K^{(0)} \rangle = 0 \quad \text{and} \quad g_K^{(0)} = 0,$$

$O(\varepsilon)$ terms:

$$\partial_t \rho^{(0)} - \partial_x \left(\frac{1}{3\sigma}(1-h)\partial_x \rho^{(0)}\right) + \partial_x \langle v g_K^{(1)} \rangle = 0 \quad \text{and} \quad g_K^{(1)} = -\frac{1}{2\sigma} h v \partial_x \rho^{(0)}.$$

The last two relations finally give the equation

$$\partial_t \rho^{(0)} - \partial_x \left(\frac{1}{3\sigma}(1-h)\partial_x \rho^{(0)}\right) - \partial_x \left(\frac{1}{3\sigma} h \partial_x \rho^{(0)}\right) = 0,$$

which gives (4.4). ∎

Remark 4.1. The coupled model proposed in [14] for the same equation does not preserve uniform flows. The problem is not the one we mentioned in Remark 3.1, since the equilibrium distribution is linear and hence homogeneous of degree one. The problem—not noticed in [14]—is rather due to the first order correction to the density of the fluid part that gives an $O(\varepsilon^2)$ error in the uniform flow preservation. However, this did not appear in the numerical tests, since this error term appears only in the fluid zone, where ε is small.

4.2. A nonlinear example: The radiative heat transfer model.

4.2.1. The model and its diffusion limit. For simplicity, we consider the radiative transfer equation including heat transfer but without photon scattering. Moreover, only a one-band approximation is considered, in the one-dimensional slab geometry (see [25]).

We denote by $I = I(t, x, \mu)$ the radiative intensity at time t, at position x in the direction whose angle with axis Ox has cosine μ. Moreover, $T(t, x)$ is the temperature of the medium. In the diffusion scaling, the equations are

$$\varepsilon^2 \partial_t T^\varepsilon - \varepsilon^2 \partial_{xx} T^\varepsilon = -\sigma(B(T^\varepsilon) - [I^\varepsilon]), \tag{4.12}$$

$$\varepsilon^2 \partial_t I^\varepsilon + \varepsilon \mu \partial_x I^\varepsilon = \sigma(B(T^\varepsilon) - I^\varepsilon), \tag{4.13}$$

where $[I]$ is the total intensity

$$[I] = \frac{1}{2} \int_{-1}^{1} I(t, x, \mu)\, d\mu,$$

and $B(T)$ is the black-body intensity

$$B(T) = T^4.$$

We also prescribe initial values

$$T^\varepsilon|_{t=0} = T_{init} \quad \text{and} \quad I^\varepsilon|_{t=0} = I_{init}.$$

These equations do not have exactly the same form as (2.1), but our method applies with very slight modifications. First, note that despite the fact that the collision operator has no conservation property, the quantity $m(\mu) = 1$ is locally conserved if we consider (4.12) and (4.13). Namely, we have the so-called energy conservation equation

$$\varepsilon \partial_t (T^\varepsilon + [I^\varepsilon]) + \partial_x (-\varepsilon \partial_x T^\varepsilon + [\mu I^\varepsilon]) = 0. \tag{4.14}$$

The equilibrium states for this model are couples (T_{eq}, I_{eq}) such that $I_{eq} = B(T_{eq})$. Note that this implies that $[\mu I_{eq}] = 0$, which justifies using a diffusion scaling.

Consequently, the micro-macro decomposition is here the following:

$$I^\varepsilon = B(T^\varepsilon) + g^\varepsilon, \tag{4.15}$$

where T^ε is kept untouched. Then the equations for g^ε and T^ε are obtained by using (4.13) and (4.14):

$$\varepsilon \partial_t (T^\varepsilon + B(T^\varepsilon)) + \partial_x (-\varepsilon \partial_x T^\varepsilon + [\mu g^\varepsilon]) = -\varepsilon \partial_t [g^\varepsilon], \tag{4.16}$$

$$\varepsilon^2 \partial_t g^\varepsilon + \varepsilon \mu \partial_x g^\varepsilon = -\sigma g^\varepsilon - (\varepsilon^2 \partial_t + \varepsilon \mu \partial_x) B(T^\varepsilon), \tag{4.17}$$

with initial data

$$T^\varepsilon|_{t=0} = T_{init} \quad \text{and} \quad g^\varepsilon|_{t=0} = I_{init} - B(T_{init}).$$

This is indeed a system similar to (2.6)–(2.7) adapted to the radiative transfer setting. An important difference is that the micro-macro decomposition (4.15) does not imply that $[g^\varepsilon] = 0$, hence the source term in (4.16).

Note that a similar idea has been used in [25] in order to derive an asymptotic preserving discretization. But the decomposition they use is a bit more complicated, since it makes use of an additional unknown that we do not need here.

Now the diffusion limit of (4.12)–(4.13) is obtained by inserting the Hilbert expansions $T^\varepsilon = T^{(0)} + \varepsilon T^{(1)} + O(\varepsilon^2)$ and $g^\varepsilon = g^{(0)} + \varepsilon g^{(1)} + O(\varepsilon^2)$ into (4.16)–(4.17). We identify terms of equal power of ε to find

$O(1)$ terms: $\quad \partial_x[\mu g^{(0)}] = 0 \quad$ and $\quad g^{(0)} = 0,$

$O(\varepsilon)$ terms:

$$\partial_t(T^{(0)} + B(T^{(0)})) + \partial_x(-\partial_x T^{(0)} + [\mu g^{(1)}]) = 0 \quad \text{and} \quad g^{(1)} = -\frac{1}{\sigma}\mu\partial_x B(T^{(0)}).$$

The last two relations give the following nonlinear diffusion equation:

$$\partial_t(T^{(0)} + B(T^{(0)})) - \partial_x\left(\partial_x T^{(0)} + \frac{1}{3\sigma}\partial_x B(T^{(0)})\right) = 0. \tag{4.18}$$

4.2.2. The micro-Macro model. As in section 2.4, we obtain the following coupled equations for T^ε, $g_K^\varepsilon = hg^\varepsilon$, $g_F^\varepsilon = (1-h)g^\varepsilon$:

(4.19)
$$\varepsilon\partial_t(T^\varepsilon + B(T^\varepsilon)) + \partial_x(-\varepsilon\partial_x T^\varepsilon + [\mu g_K^\varepsilon] + [\mu g_F^\varepsilon]) = -\varepsilon\partial_t[g_K^\varepsilon] - \varepsilon\partial_t[g_F^\varepsilon],$$

(4.20)
$$\varepsilon^2\partial_t g_K^\varepsilon + \varepsilon h\mu\partial_x g_K^\varepsilon + \varepsilon h\mu\partial_x g_F^\varepsilon = -\sigma g_K^\varepsilon - h(\varepsilon^2\partial_t + \varepsilon\mu\partial_x)B(T^\varepsilon),$$

(4.21)
$$\varepsilon^2\partial_t g_F^\varepsilon + \varepsilon(1-h)\mu\partial_x g_F^\varepsilon + \varepsilon(1-h)\mu\partial_x g_K^\varepsilon = -\sigma g_F^\varepsilon - (1-h)(\varepsilon^2\partial_t + \varepsilon\mu\partial_x)B(T^\varepsilon),$$

with initial data

$$T^\varepsilon|_{t=0} = T_{init}, \quad g_K^\varepsilon|_{t=0} = h(I_{init} - B(T_{init})), \quad g_F^\varepsilon|_{t=0} = (1-h)(I_{init} - B(T_{init})).$$

Now we aim to perform the diffusion approximation for g_F^ε in (4.19) and in (4.21). However, it turns out that the term $\partial_t[g_K^\varepsilon]$ in (4.19) leads to an asymptotic model that does not have the good properties. Actually, it is better to replace this term by its value given by (4.20). This yields the following equation:

(4.22)
$$\varepsilon\partial_t(T^\varepsilon + (1-h)B(T^\varepsilon) + [g_F^\varepsilon]) - \varepsilon\partial_{xx}T^\varepsilon + (1-h)(\partial_x[\mu g_K^\varepsilon] + \partial_x[\mu g_F^\varepsilon]) = \frac{1}{\varepsilon}\sigma[g_K^\varepsilon].$$

Then using exactly the same arguments as in section 4.1.2, we perform the diffusion approximation for g_F^ε in (4.22) rewritten as

$$\begin{aligned}&\varepsilon\partial_t[g_F^\varepsilon] + (1-h)\partial_x[\mu g_F^\varepsilon]\\ &\qquad = -\varepsilon\partial_t(T^\varepsilon + (1-h)B(T^\varepsilon)) + \frac{1}{\varepsilon}\sigma[g_K^\varepsilon] - (1-h)\partial_x[\mu g_K^\varepsilon] + \varepsilon\partial_{xx}T^\varepsilon,\end{aligned} \tag{4.23}$$

where every term of the right-hand side is considered to be an $O(\varepsilon)$, and also in (4.21) rewritten as

(4.24)
$$\varepsilon^2\partial_t g_F^\varepsilon + \varepsilon(1-h)\mu\partial_x g_F^\varepsilon + \sigma g_F^\varepsilon = -\varepsilon(1-h)\mu\partial_x g_K^\varepsilon - (1-h)(\varepsilon^2\partial_t + \varepsilon\mu\partial_x)B(T^\varepsilon),$$

where the term involving g_K^ε is assumed to be an $O(\varepsilon^2)$.

Then inserting the Hilbert expansions $T^\varepsilon = T^{(0)} + \varepsilon T^{(1)} + O(\varepsilon^2)$ and $g_F^\varepsilon = g_F^{(0)} + \varepsilon g_F^{(1)} + O(\varepsilon^2)$ into (4.23) and (4.24), we find the relations

$O(1)$ terms: $\quad (1-h)\partial_x[\mu g_F^{(0)}] = 0 \quad$ and $\quad g_F^{(0)} = 0,$

$O(\varepsilon)$ terms:

$$(1-h)\partial_x[\mu g_F^{(1)}] = -\partial_t\Big(T^{(0)} + (1-h)B(T^{(0)})\Big) + \frac{1}{\varepsilon^2}\sigma[g_K^\varepsilon] - (1-h)\partial_x\frac{1}{\varepsilon}[\mu g_K^\varepsilon] + \partial_{xx}T^{(0)}$$

and $\quad g_F^{(1)} = -\dfrac{1}{\sigma}(1-h)\mu\partial_x B(T^{(0)}).$

The last two relations then give a diffusion equation for $T^{(0)}$ coupled with the kinetic equation (4.20) for g_K^ε. This is our micro-Macro model that finally reads

$$\varepsilon^2\partial_t(T^\varepsilon + (1-h)B(T^\varepsilon)) - \varepsilon^2\partial_{xx}T^\varepsilon - \varepsilon^2(1-h)\partial_x\left((1-h)\frac{1}{3\sigma}\partial_x B(T^\varepsilon)\right)$$

$$+ \varepsilon(1-h)\partial_x[\mu g_K^\varepsilon] = \sigma[g_K^\varepsilon], \tag{4.25}$$

$$\varepsilon^2\partial_t g_K^\varepsilon + \varepsilon h\mu\partial_x g_K^\varepsilon + \varepsilon h\mu\partial_x g_F^\varepsilon = -\sigma g_K^\varepsilon - h(\varepsilon^2\partial_t + \varepsilon\mu\partial_x)B(T^\varepsilon), \tag{4.26}$$

with $g_F^\varepsilon = -\varepsilon(1-h)\frac{1}{\sigma}\mu\partial_x B(T^\varepsilon)$ and the initial data

$$T^\varepsilon|_{t=0} = T_{init}, \quad g_K^\varepsilon|_{t=0} = h(I_{init} - B(T_{init})).$$

Again, note that $T^{(0)}$ is denoted T^ε in this model, since it still depends on ε through the coupling.

As we noticed for the micro-Macro models in the previous sections, this model gives well the original radiative heat transfer equation (4.12)–(4.13) in the kinetic zone (where $h = 1$) and the nonlinear diffusion model (4.18) in the fluid zone (where $h = 0$).

4.2.3. Properties of the micro-Macro model. We can now prove that our micro-Macro model satisfies the following interesting properties.

PROPOSITION 4.2.

(i) *Preservation of uniform flows.*

If the initial condition (T_{init}, I_{init}) is a constant equilibrium (i.e., such that $I_{init} = B(T_{init})$), then $T = T_{init}$ and $g_K = h(I_{init} - B(T_{init})) = 0$ are solutions of the micro-Macro model (4.25)–(4.26)*, and $(T, B(T) + g_K) = (T_{init}, B(T_{init}))$; that is, the kinetic/fluid solution of the micro-Macro model is exactly the solution of the original kinetic model.*

(ii) *Full diffusion limit.*

As ε goes to zero, the solution $(T^\varepsilon, g_K^\varepsilon)$ of the micro-Macro model converges to $(T^{(0)}, 0)$, where $T^{(0)}$ is a solution of the nonlinear diffusion equation (4.18)*.*

Proof. Again, the proof of (i) is very similar to that of Proposition 3.2 and is left to the reader. For (ii), we insert the Hilbert expansions $T^\varepsilon = T^{(0)} + \varepsilon T^{(1)} + O(\varepsilon^2)$ and $g_F^\varepsilon = g_F^{(0)} + \varepsilon g_F^{(1)} + O(\varepsilon^2)$ into (4.26) and into the following energy conservation relation obtained by averaging the sum of (4.25) and (4.26):

$$\varepsilon\partial_t(T^\varepsilon + B(T^\varepsilon)) + \varepsilon\partial_t[g_K^\varepsilon] - \varepsilon\partial_x\left(\partial_x T^\varepsilon + (1-h)\frac{1}{3\sigma}\partial_x B(T^\varepsilon)\right) + \partial_x[\mu g_K^\varepsilon] = 0.$$

By identifying terms of equal power of ε, we obtain relations

$$O(1) \text{ terms:} \quad \partial_x[\mu g_K^{(0)}] = 0 \quad \text{and} \quad g_K^{(0)} = 0,$$

$O(\varepsilon)$ terms:

$$\partial_t(T^{(0)} + B(T^{(0)})) - \partial_x\left(\partial_x T^{(0)} + (1-h)\frac{1}{3\sigma}\partial_x B(T^{(0)})\right) + \partial_x[\mu g_K^{(1)}] = 0$$

$$\text{and} \quad g_K^{(1)} = -h\frac{1}{\sigma}\mu\partial_x B(T^{(0)}).$$

The last two relations give nonlinear diffusion equation (4.18). ∎

Remark 4.2. This model is a typical example for which the coupling method of [14] does not possess the property of preservation of uniform flows. The main reason is that as found in [15], the equilibrium state $I = B(T)$ is not homogeneous of degree one with respect to T. Namely, in the coupling of [14], we need that $B(hT) = hB(T)$, which is obviously not true.

5. Numerical approximations. Here we briefly present how the previous micro-Macro models have been discretized for the numerical tests of section 6. To avoid too large a number of numerical results, we do not solve the micro-Macro model for the linear transport equation of section 4.1.

The main characteristics of our discretizations are the following. First, the time variable t is discretized with nodes $t_n = n\Delta t$ for $n \geq 0$, the space variable x is discretized with mesh points $x_i = i\Delta x$ for $i = 1, \ldots, i_{max}$, and we define i_a and i_b such that $x_{i_a} = a$ and $x_{i_b} = b$. We set $h_i = h(x_i)$, $\rho_i = \rho(t_n, x_i)$, and $g_{K,i}^n = g_K(t_n, x_i)$. The velocity variable v (or μ) is discretized with nodes $v_j = j\Delta v$, but for more clarity we do not use the subscript j in what follows. The integrals in the fluxes and in the collision operators are approximated by a simple rectangle formula.

It is rather difficult to analyze the structure of our micro-Macro systems (3.8)–(3.9), (4.25)–(4.26). In particular the discretization of the material derivative of the local equilibrium on the right-hand side of the kinetic equation is an important issue. Here we propose a simple approach, yet without rigorous numerical analysis.

First, we recall that the initial step to obtain our models was to rewrite the original kinetic equation (2.1) as the equivalent system (2.6)–(2.7) by using the micro-macro decomposition (2.4). Therefore it is natural to design a simple scheme for (2.1) and then to use the micro-macro decomposition (2.4) to obtain a numerical scheme for (2.6)–(2.7). Namely, we discretize (2.1) with the following usual first order explicit upwind approximation:

$$\frac{f_i^{n+1} - f_i^n}{\Delta t} + \frac{\phi_{i+\frac{1}{2}}(f^n) - \phi_{i-\frac{1}{2}}(f^n)}{\Delta x} = Q(f_i^n), \tag{5.1}$$

with the numerical flux

$$\phi_{i+\frac{1}{2}}(f) = v^- f_{i+1} + v^+ f_i. \tag{5.2}$$

We can also use standard second order approximation with slope limiters. Under a classical time step restriction, this scheme has many strong properties, such as stability in various norms. By using the micro-macro decomposition (2.4), we deduce from (5.1) the following numerical discretization of (2.6)–(2.7):

$$\frac{\rho_i^{n+1} - \rho_i^n}{\Delta t} + \frac{\Psi_{i+\frac{1}{2}}^n - \Psi_{i-\frac{1}{2}}^n}{\Delta x} = 0, \tag{5.3}$$

$$\frac{g_i^{n+1} - g_i^n}{\Delta t} + \frac{\phi_{i+\frac{1}{2}}(g^n) - \phi_{i-\frac{1}{2}}(g^n)}{\Delta x} = \frac{1}{\varepsilon}Q(E[\rho_i^n] + g_i^n) - S_i^n, \tag{5.4}$$

where $\Psi^n_{i+\frac12}$ is a consistent approximation of $\Psi(\rho^n, g^n) = F(\rho^n) + \langle vmg^n\rangle$ at $x_{i+\frac12}$, and S^n_i denotes the discretization of the downscaling term $(\partial_t + v\partial_x)E[\rho]$ defined by

$$S^n_i = \frac{E[\rho^{n+1}_i] - E[\rho^n_i]}{\Delta t} + \frac{\phi_{i+\frac12}(E[\rho^n]) - \phi_{i-\frac12}(E[\rho^n])}{\Delta x}. \tag{5.5}$$

By equivalence with (5.1), this scheme is perfectly stable.

Now, in order to obtain a numerical discretization of our micro-Macro models, a natural idea is to mimic the derivation of the models on the numerical scheme (5.3)–(5.4) (namely, splitting of g by using the transition function h and then localization). While this works very well for the hyperbolic case, we prefer to use another approach for the parabolic case. These constructions are detailed in the following sections.

5.1. Micro-Macro model for the general hydrodynamic scaling (section 3). By applying the same procedure as described in sections 2.4 and 3 to the numerical scheme (5.3)–(5.4), we obtain the following approximation of our model (for completeness, the micro-Macro model is recalled before we give the numerical scheme).

The model.

$$\partial_t\rho + \partial_x F(\rho) + \partial_x\langle vmg_K\rangle = 0,$$
$$\partial_t g_K + hv\partial_x g_K = \frac{1}{\varepsilon}hQ(E[\rho] + g_K) - h(\partial_t + v\partial_x)E[\rho].$$

The scheme.

$$\frac{\rho^{n+1}_i - \rho^n_i}{\Delta t} + \frac{\Psi^n_{i+\frac12} - \Psi^n_{i-\frac12}}{\Delta x} = 0, \tag{5.6}$$

$$\frac{g^{n+1}_{K,i} - g^n_{K,i}}{\Delta t} + h_i\frac{\phi_{i+\frac12}(g^n_K) - \phi_{i-\frac12}(g^n_K)}{\Delta x} = \frac{1}{\varepsilon}h_iQ(E[\rho^n_i] + g^n_{K,i}) - h_iS^n_i. \tag{5.7}$$

Of course, this scheme is no longer equivalent to the numerical approximation of the original kinetic equation. Consequently, we cannot prove any stability property for the moment. However, note that in fluid zones ($h = 0$) and in kinetic zones ($h = 1$), we recover two schemes that are stable. Moreover, we will show in section 6 that our scheme behaves very well even where $0 < h < 1$.

Now, following a standard method (see [10, 21, 30]), we briefly explain how this scheme can be extended to second order in space. We simply assume that the flux Ψ can be split into a positive and a negative part $\Psi = \Psi^+ + \Psi^-$. The first and second order reconstructions of the positive flux are obtained by the following piecewise polynomial $\Psi^+(x)$:

$$\Psi^+(x) = \Psi^+(\rho_i, g_{K,i}) + s_i(x - x_i), \qquad x \in [x_{i+\frac12}, x_{i-\frac12}].$$

This equality must be understood componentwise; that is, we have one slope s_i per component of the flux. The possible spurious oscillations near discontinuities are suppressed by the classical minmod slope limiter

$$s_i = \frac{1}{\Delta x}\operatorname{minmod}\Big(\Psi^+(\rho_{i+1}, g_{K,i+1}) - \Psi^+(\rho_i, g_{K,i}), \Psi^+(\rho_i, g_{K,i}) - \Psi^+(\rho_{i-1}, g_{K,i-1})\Big),$$

while taking $s_i = 0$ gives a first order scheme. We can do the same reconstruction for the negative flux. Then the numerical flux $\Psi_{i+\frac12}$ is computed by upwinding and by using the previous splitting

$$\Psi^n_{i+\frac12} = \Psi^+_i(x_{i+\frac12}) + \Psi^-_{i+1}(x_{i+\frac12}).$$

Finally, the splitting of Ψ is naturally derived from its kinetic formulation

$$\begin{aligned}\Psi(\rho, g_K) &= F(\rho) + \langle vmg_K\rangle \\ &= \langle vm(E[\rho] + g_K)\rangle \\ &= \langle v^+ m(E[\rho] + g_K)\rangle + \langle v^- m(E[\rho] + g_K)\rangle.\end{aligned}$$

For the equilibrium part, this is nothing but the kinetic flux vector splitting introduced by Mandal and Deshpande in [31] for the Euler equations of gas dynamics. We can also use the flux vector splitting of Perthame [34], where the physical equilibrium is replaced in the splitting of Ψ by a compactly supported square-shaped distribution.

By applying the same analysis as in section 3.1, it is rather simple to prove that this scheme preserves uniform flows.

5.2. Asymptotic preserving scheme for relaxation kinetic equations. This scheme can be directly applied to the BGK and the Jin–Xin models. But in these cases, the collision operator is linear and can be taken implicit. This avoids a severe CFL condition due to the collision frequency and gives schemes that are asymptotic preserving, as explained hereinafter. Indeed, with the explicit time discretization of the collision operator given above, small ε create large negative contributions to $g_{K,i}^{n+1}$. This can be controlled only if Δt is small enough, say $\Delta t < \varepsilon\tau$. Since relaxation collision operators simply write $Q(E[\rho]+g) = -\frac{1}{\tau}g$, they can easily be taken implicit, which gives instead of (5.7) the relation

$$\frac{g_{K,i}^{n+1} - g_{K,i}^n}{\Delta t} + h_i \frac{\phi_{i+\frac{1}{2}}(g_K^n) - \phi_{i-\frac{1}{2}}(g_K^n)}{\Delta x} = -\frac{1}{\varepsilon\tau} g_{K,i}^{n+1} - h_i S_i^n. \tag{5.8}$$

In this case, it seems clear that there is no more positivity issue due to ε and that Δt can be taken independent of ε. In particular, one can formally pass to the limit $\varepsilon = 0$ in this relation (with constant Δt and Δx) to find $g_{K,i}^{n+1} = 0$. Passing to the limit in the discrete macroscopic relation (5.6) gives a scheme for the asymptotic hyperbolic model (3.2). A scheme with such a property is often called an "asymptotic preserving scheme."

Actually this can be rigorously proved if $h_i = 1$. In this case relation (5.6) and (5.8) are strictly equivalent to

$$\frac{f_i^{n+1} - f_i^n}{\Delta t} + \frac{\phi_{i+\frac{1}{2}}(f^n) - \phi_{i-\frac{1}{2}}(f^n)}{\Delta x} = \frac{1}{\varepsilon\tau}(E[\rho_i^{n+1}] - f_i^{n+1}),$$

which is an implicit discretization of the full relaxation kinetic equation. Thus it is well known that this scheme is L^∞ stable uniformly with respect to ε.

If $h_i \neq 1$, a rigorous proof seems unlikely, while our numerical results show that the scheme is still stable in this case. However, by using the same kind of arguments as in section 3.2, this may be understood as follows. Assume the buffer is located inside the fluid zone (where ε is small). This means that where $h_i \neq 1$, we have from (5.8) that $g_{K,i}^n$ is an $O(\varepsilon)$, hence a very small quantity. Outside the buffer zone, $h_i = 0$, and then $g_{K,i}^n$ is zero. Consequently, the possible instabilities should remain of size ε and located inside the buffer.

Finally, note that even with this technique, the time step is still constrained by the maximum molecular velocity, which can be very different from the fluid time scale (given by the macroscopic velocity). In such a case, we could apply a technique used in [14]: a time stepping algorithm is used to advance differently the macroscopic and

kinetic parts when necessary. If the time step Δt_K imposed by the kinetic part is much lower than the time step Δt_F due to the fluid part, we solve the kinetic equation during $N = [\Delta t_F/\Delta t_K]$ time steps Δt_K with a constant fluid contribution. Then the fluid equation is solved with time step Δt_F. Note that we did not need to use this technique in our tests.

5.3. Micro-Macro model model for the heat transfer equation (section 4.2). In this case, we find it not very convenient to derive a numerical scheme from (5.3)–(5.4). Indeed, this leads to complex discretizations as five point stencils for the diffusion terms. Instead we directly discretize the micro-Macro model by standard finite difference approximations (three point stencil for second order derivatives and first order one-sided approximation for the transport operators). We rewrite below the micro-Macro model we found, and we give the corresponding numerical approximation we use.

The model.

$$\partial_t(T + (1-h)B(T)) - \partial_{xx}T - (1-h)\partial_x\left((1-h)\frac{1}{3\sigma}\partial_x B(T)\right) + (1-h)\partial_x[\mu g_K] = \sigma[g_K],$$

$$\partial_t g_K + h\mu\partial_x g_K - h\mu^2\partial_x\left((1-h)\frac{1}{\sigma}\partial_x B(T)\right) = -\sigma g_K - h(\partial_t + \mu\partial_x)B(T).$$

The scheme.

$$(1 + (1-h_i)B'(T_i^n))\frac{T_i^{n+1} - T_i^n}{\Delta t} - \frac{T_{i+1}^n - 2T_i^n + T_{i-1}^n}{\Delta x^2} - (1-h_i)\frac{1}{\Delta x}\left(\left(\frac{1-h}{3\sigma}\right)_{i+\frac{1}{2}}\frac{B(T_{i+1}^n) - B(T_i^n)}{\Delta x} - \left(\frac{1-h}{3\sigma}\right)_{i-\frac{1}{2}}\frac{B(T_i^n) - B(T_{i-1}^n)}{\Delta x}\right) + (1-h_i)\left[\frac{\phi_{i+\frac{1}{2}}(g_K^n) - \phi_{i-\frac{1}{2}}(g_K^n)}{\Delta x}\right] = \sigma_i[g_{K,i}^n], \tag{5.9}$$

$$\frac{g_{K,i}^{n+1} - g_{K,i}^n}{\Delta t} + h_i\frac{\phi_{i+\frac{1}{2}}(g_K^n) - \phi_{i-\frac{1}{2}}(g_K^n)}{\Delta x} + h_i\mu^2\frac{1}{\Delta x^2}\left(\left(\frac{1-h}{\sigma}\right)_{i+\frac{1}{2}}\frac{B(T_{i+1}^n) - B(T_i^n)}{\Delta x} - \left(\frac{1-h}{\sigma}\right)_{i-\frac{1}{2}}\frac{B(T_i^n) - B(T_{i-1}^n)}{\Delta x}\right) = -\sigma_i g_{K,i}^n - h_i S_i^n. \tag{5.10}$$

For clarity, we have dropped ε in these relations. Again, by applying the same analysis as in section 3.1, it is rather simple to prove that this scheme preserves uniform flows.

On the contrary, it is much more difficult to design an asymptotic preserving scheme here. Actually, the stiffness of the equations is due not only to the collision operator but also to the transport terms. We defer the design of an adapted asymptotic preserving scheme to a future work. For instance, it should be possible to extend the asymptotic preserving scheme of [25] to this model. We refer the reader to [14] for another example of such a scheme applied to a different kinetic/diffusion coupled model.

6. Numerical results. In this section, we want to illustrate the properties and potentialities of our method with simple one-dimensional (1D) cases. Our goal is mainly twofold:

- to confirm the robustness and stability of our method;
- to test its accuracy and to show how it can be used to approximate a kinetic model when a large part of the domain is close to an equilibrium state.

We shall first consider the Jin–Xin relaxation approximation (3.16) of the Burgers equation. Then we shall use two 1D BGK models similar to (3.14), where the second one accounts for three-dimensional (3D) effects in velocity. Finally, we shall test our method on the radiative heat transfer model (4.12)–(4.13).

Example 6.1. Numerical solution of the micro-Macro model for the Jin–Xin relaxation approximation (3.16) of the Burgers equation.

In the first test, we want to prove that the oscillation observed in [15] (and due to the nonpreservation of uniform flows) is not created by our new method.

Here we take $\varepsilon = 0.01$. We use 100 points to solve the kinetic model (3.16) in the entire domain and 100 points for the numerical approximation of the micro-Macro model. The function h is defined to be piecewise linear and continuous: 0 for $x \le a$, 1 for $x \ge b$, and linear between a and b. We use two choices of buffer zones: $a = -0.1$, $b = 0.1$; $a = -0.05$, $b = 0.05$, respectively.

In the different figures, the kinetic solution $\rho = f_1 + f_2$ is plotted with a solid line, while the density of the micro-Macro model ρ is shown by the symbol "o." We also plot the exact solution for the full hydrodynamic limit—that is, the Burgers equation in this case—with a dash-dotted line. The buffer zone is made clearly visible by two vertical dotted lines at $x = a$ and $x = b$.

We consider a shock wave corresponding to the initial condition: $\rho = 1$ in $[-0.5, 0]$ and $\rho = 0.5$ in $[0, 0.5]$. We observe (Figures 1–2) that the micro-Macro model is very close to the kinetic solution in the whole domain. As expected, there is no oscillation at all.

In a second test, we want to validate our method in a situation more adapted to the derivation of our model. Consequently, (3.16) is considered with a relaxation time τ that depends on x instead of the single parameter ε. This relaxation time is chosen to be 0.001 for $x \le -0.0505$ (fluid domain), 0.1 for $x \ge 0.101$ (kinetic domain), and linear between -0.0505 and 0.101. Following the analysis given in section 3.2, we choose a buffer zone located inside the fluid zone. Namely, we take $a = -0.202$ and $b = 0.202$, with h defined as in the previous test. The initial condition is again a shock wave but corresponding to the new initial condition: $\rho = 1$ in $[0, -0.1667]$ and $\rho = 0.5$ in $[0.1667, 1]$ (that is, the initial discontinuity is located at the first third of the domain). For the discretization, we use the second order scheme of section 5.1 with 100 points.

In Figures 3 and 4, the same symbols as in the previous test are used, we plot the same quantities, and we materialize by dotted lines the fluid and kinetic domains (with the corresponding values of the relaxation time). We plot our results for four different times. First, we globally note that the micro-Macro model is really very close to the full kinetic model. More precisely, when the shock is inside the fluid zone (Figure 3(top)), the micro-Macro model is slightly different from the kinetic model, since only the fluid equation is solved here. However, the three models are very close in this zone. As the shock reaches the kinetic zone, the hydrodynamic solution becomes very different, while the micro-Macro and the kinetic models remain very close (almost indistinguishable in the figures). Consequently, our micro-Macro model behaves fairly well on this test case.

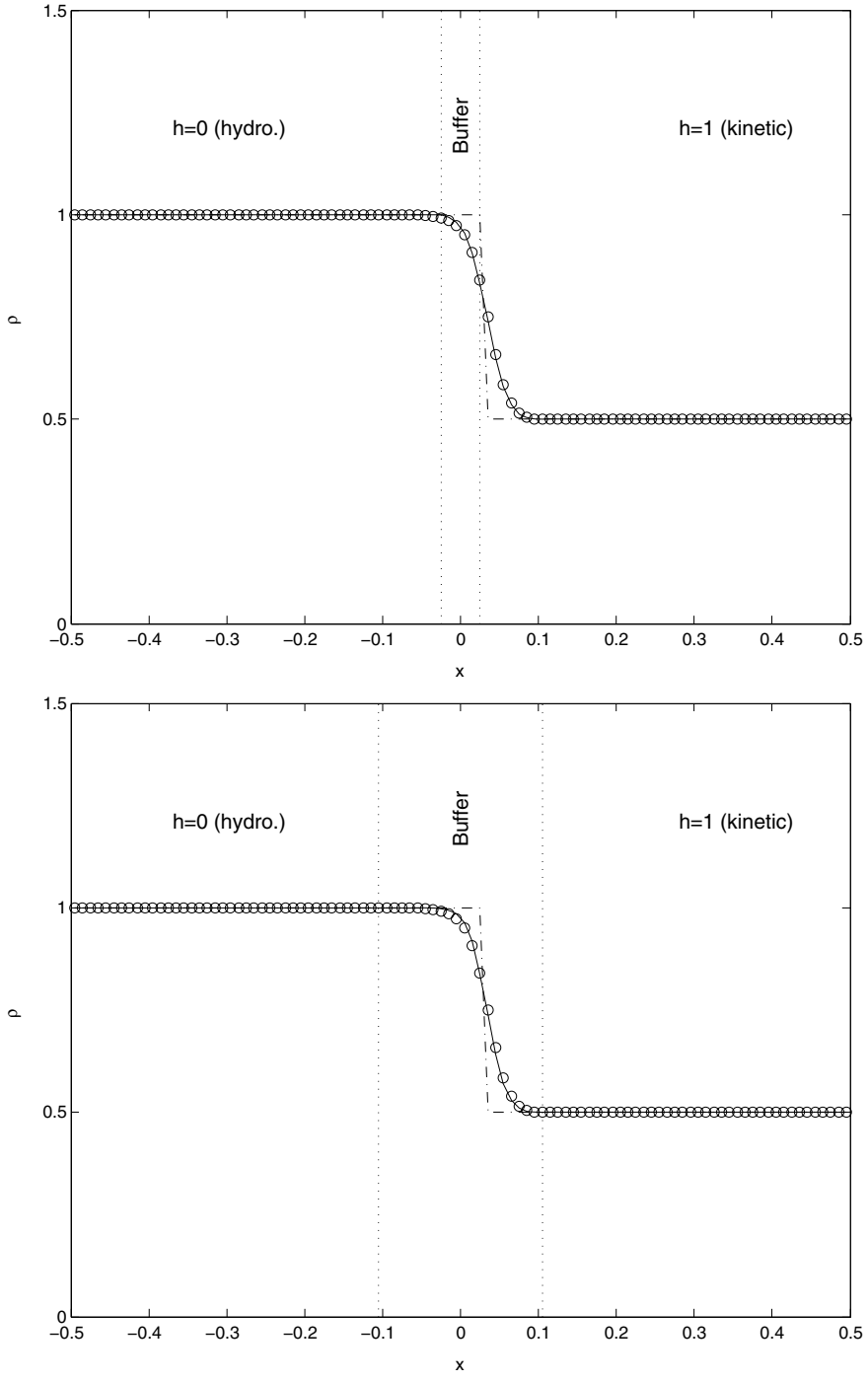

FIG. 1. *The numerical solution of* ρ *for the Jin–Xin relaxation model* (3.16) *with* $\varepsilon = 0.01$ *at* $t = 0.0450$ *for the shock initial condition, with narrow (top) and large (bottom) buffer zone. The solid line is the numerical solution of model* (3.16)*, while* "o" *is the numerical solution of the micro-Macro model (*1000 *grid points), and* ".-" *is the exact solution for the Burgers equation (full hydrodynamic limit).*

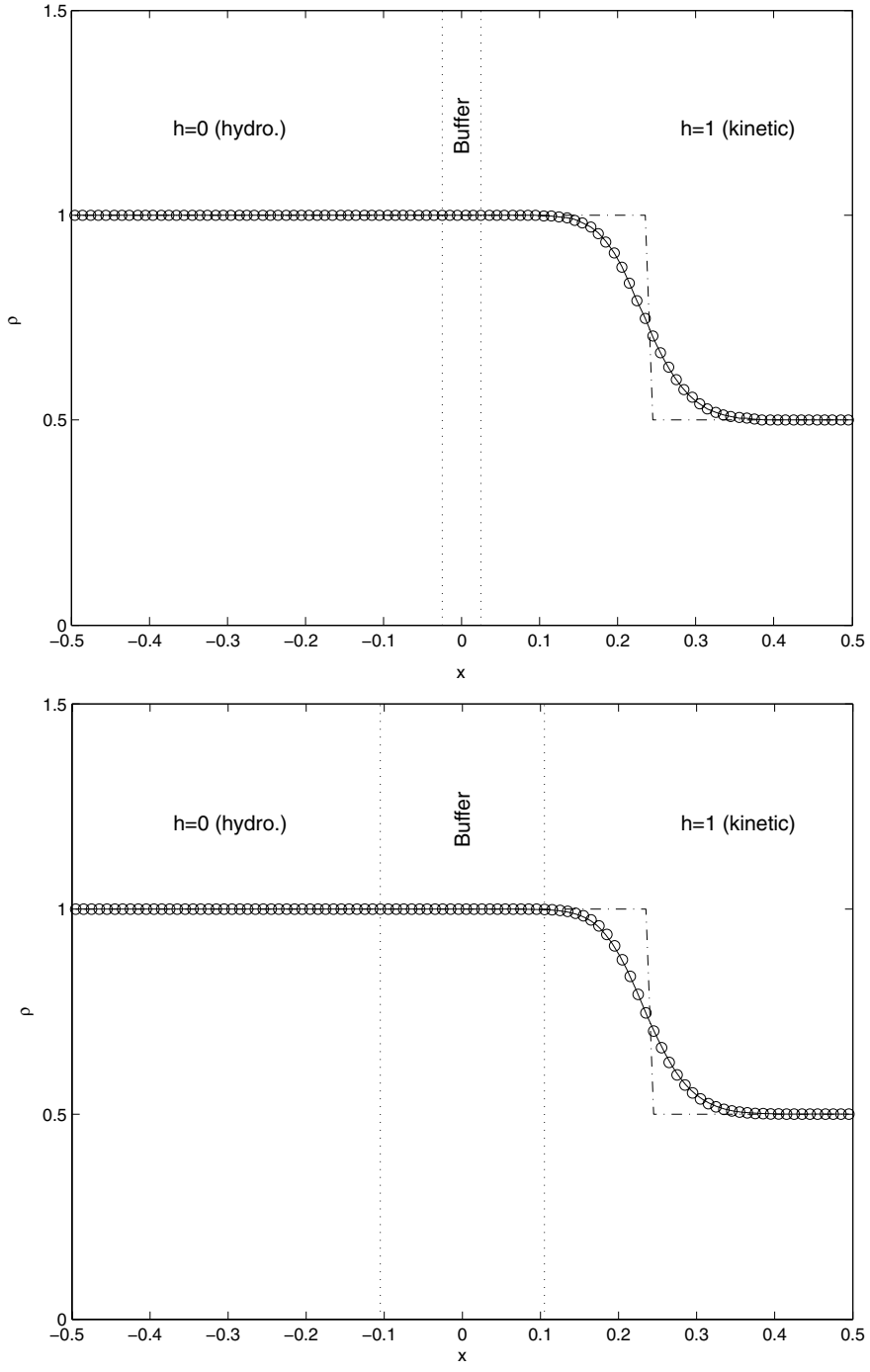

FIG. 2. *The numerical solution of* ρ *for the Jin–Xin relaxation model* (3.16) *with* $\varepsilon = 0.01$ *at* $t = 0.350$ *for the shock initial condition, with narrow (top) and large (bottom) buffer zone. The solid line is the numerical solution of model* (3.16)*, while* "o" *is the numerical solution of the micro-Macro model (*1000 *grid points), and* ".-" *is the exact solution for the Burgers equation (full hydrodynamic limit).*

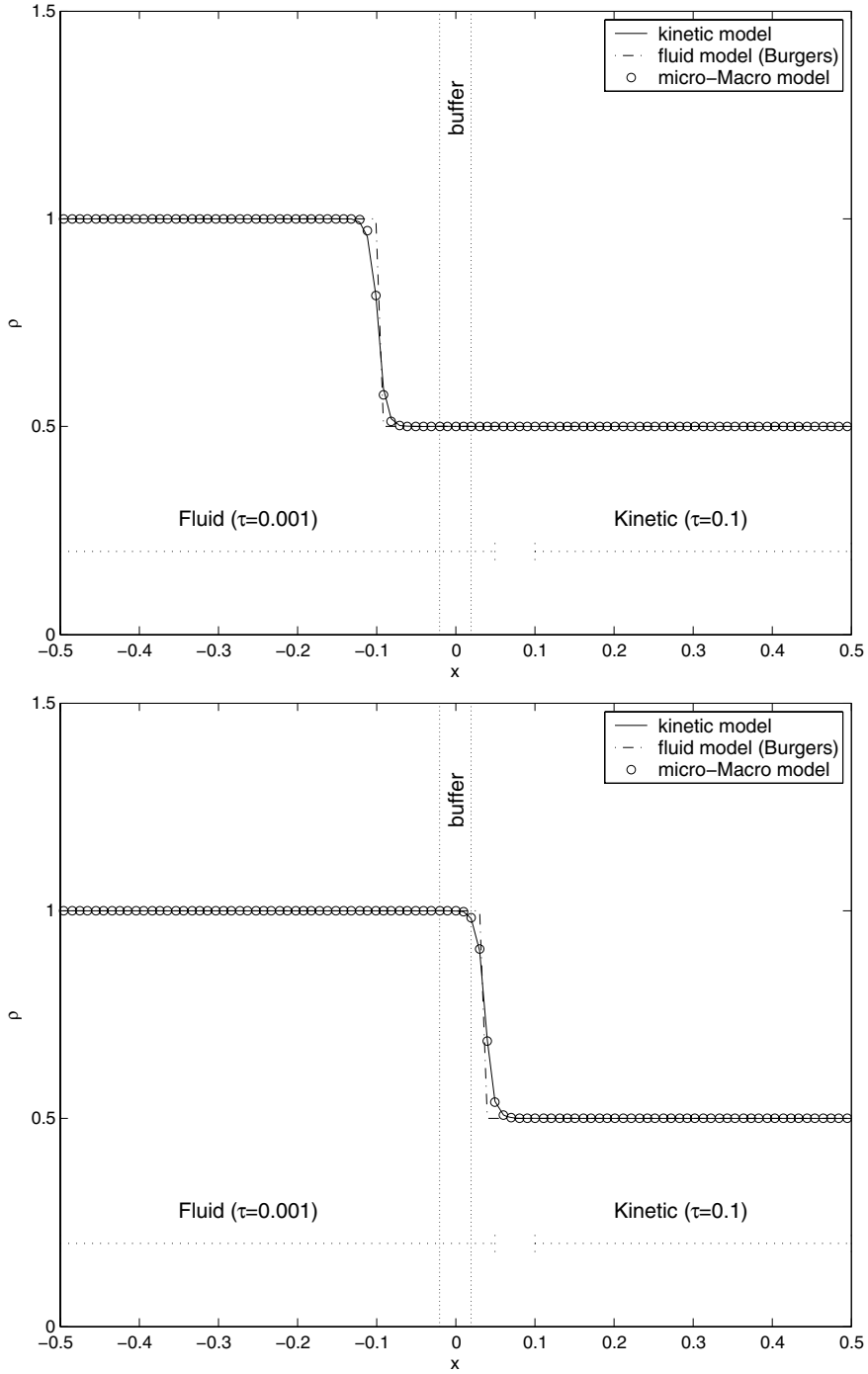

FIG. 3. *The numerical solution of ρ for the Jin–Xin relaxation model* (3.16) *with a space dependent relaxation time (from* 0.001 *to* 0.1*) at* $t = 0.0909$ *(top) and* $t = 0.2773$ *(bottom).*

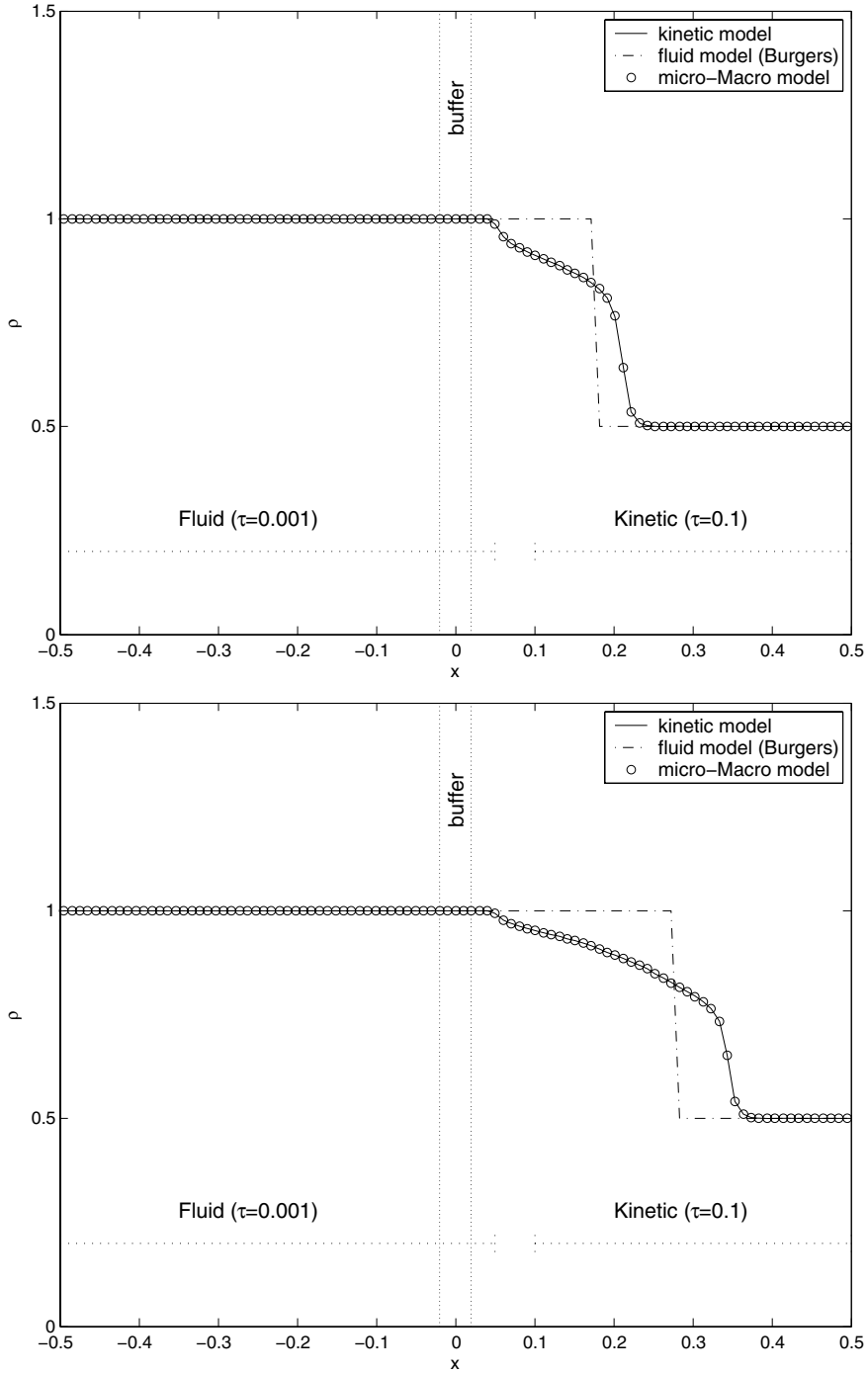

FIG. 4. *The numerical solution of ρ for the Jin–Xin relaxation model* (3.16) *with a space dependent relaxation time (from* 0.001 *to* 0.1*) at* $t = 0.4773$ *(top) and* $t = 0.5909$ *(bottom).*

Example 6.2. Numerical solution of the micro-Macro model for the 1D-1D BGK equation (3.14).

In this example, we perform a test similar to the previous one with the Xin–Jin model. We take a space dependent relaxation time τ instead of the single parameter ε such that we can clearly define a fluid zone (where τ is small) and a kinetic zone (where τ is larger). Note that to our knowledge, this model is not really physical, since in rarefied gas dynamics, the relaxation time depends on x through the macroscopic quantities only. But in that case, the definition of fluid and kinetic zones is less obvious (see Example 6.3).

We compare our micro-Macro model (3.15) to the original kinetic equation and to the full hydrodynamic limit (3.10) which is Euler equations with $\gamma = 3$. The equations are solved in the domain $[0, 1]$ with 100 points in space and second order schemes. The time step is the same for the three models and based on the CFL condition for the kinetic equation. The initial condition is a high density region of gas at rest at uniform temperature located around the middle of the domain. It is defined for the kinetic equation by a Maxwellian distribution with the macroscopic quantities density $= 1 + 0.1/\sqrt{0.002\pi}\exp(-(x - 0.5)^2/(0.002))$, velocity $= 0$, and temperature $= 1$. The fluid model is initialized with the same macroscopic data, and the micro-Macro model is initialized accordingly.

We use three different relaxation time functions and the same buffer zone [0.4950, 0.5248]. The transition function h is defined with a piecewise affine function, as in the previous example.

In the test, we use a relaxation time that varies smoothly from 0.001 to 1 with the formula $\tau(x) = 1/2(2/\pi \arctan((x - 0.5)/0.005 - 30) + 1)$. Thus in the buffer zone, τ varies between 0.0103 and 0.0127. In Figure 5, we plot the density, the velocity, and the pressure of the gas, as well as the relaxation time that allows us to see where the fluid and kinetic zones are located. Quite surprisingly, we observe that the kinetic and the fluid models are very different even in the fluid zone. It seems that the kinetic effects of the kinetic zone influence the solution as far as the fluid zone. But the micro-Macro model does not have this property, since it seems much closer to the fluid model in this zone than to the kinetic solution. On the contrary, the micro-Macro and the kinetic models are very close in the kinetic zone. It probably means that the micro-Macro model does not take into account enough kinetic effect.

Now we decrease these kinetic effects by taking a relaxation time that varies smoothly from 0.0001 to 0.1 with the formula $\tau(x) = 1/2(2/\pi \arctan((x-0.5)/0.005-30)+1)0.1$. Then the kinetic zone is rather what is called a transition regime zone in aerodynamics. We observe in Figure 6 that the micro-Macro model is now very close to the kinetic model in the whole domain.

Finally, we use a relaxation time that varies from 0.001 to 1 like in the first test but with a piecewise linear and continuous function: 0.001 for $x < 0.6$, 1 for $x > 0.7$, and linear between 0.6 and 0.7. Thus the buffer zone is clearly inside a highly fluid zone (τ is 0.001 inside, while it was around 0.01 in the first test). Again we observe in Figure 7 that the micro-Macro model is very close to the kinetic model in the whole domain.

We conclude from this test that to have an accurate approximation of the kinetic equation with our micro-Macro model, either the buffer zone must be in a real fluid zone, or the kinetic effects must be localized enough.

Example 6.3. Numerical solution of the micro-Macro model for a 1D-3D BGK model of rarefied gas dynamics.

Here we test the micro-Macro model for the following BGK model of rarefied gas

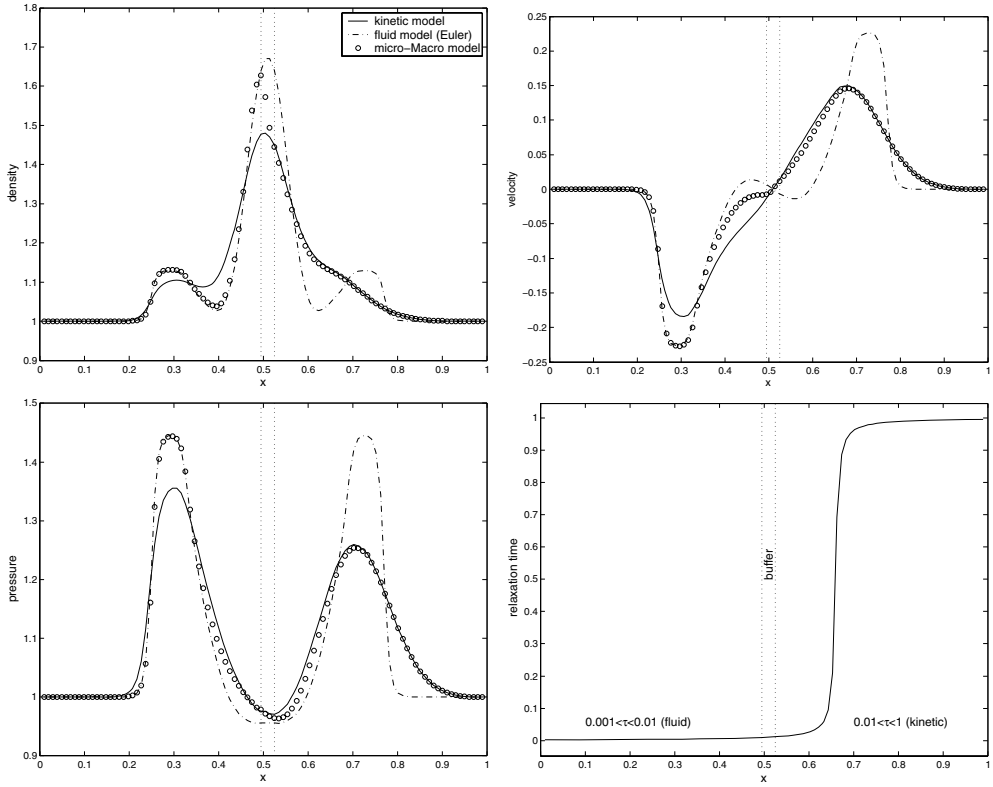

FIG. 5. *The numerical solution at* $t = 0.1103$ *of density (top left), velocity (top right), and pressure (bottom left) for the* 1*D BGK model* (3.14) *with a space dependent relaxation time (from* 0.001 *to* 1*, plotted bottom right).*

dynamics:

$$\partial_t \begin{pmatrix} F \\ G \end{pmatrix} + v\partial_x \begin{pmatrix} F \\ G \end{pmatrix} = \nu(\rho) \begin{pmatrix} M[\rho] - F \\ RTM[\rho] - G \end{pmatrix},$$

where $M[\rho] = \frac{n}{\sqrt{2\pi RT}} \exp(-\frac{(v-u)^2}{2RT})$ and

$$\rho = \left(n, nu, n\frac{u^2}{2} + \frac{3}{2}nRT \right) = \left\langle \left(1, v, \frac{1}{2}v^2 \right) F + (0,0,1)G \right\rangle.$$

The collision frequency is $\nu(\rho) = \frac{p}{\mu}$, where $p = nRT$ is the pressure and $\mu = CT^\omega$ is the viscosity. For hydrogen, we have $R = 208.24$, $C = 1.99 \times 10^{-3}$, and $\omega = 0.81$ (see [4]).

This model is 1D in space and two-dimensional (2D) in velocity, but it accounts for 3D velocity effects. It is obtained with standard reduction technique of the full 3D BGK model of rarefied gas dynamics (see [20]). Namely, $F(v) = \int_{\mathbb{R}\times\mathbb{R}} f(v, v_y, v_z)\, dv_y dv_z$ and $G(v) = \int_{\mathbb{R}\times\mathbb{R}} \frac{1}{2}(v_y^2 + v_z^2) f(v, v_y, v_z)\, dv_y dv_z$, where f is the full distribution function. This model is of the form (2.1), and its hydrodynamic limit is the Euler system of gas dynamics for monatomic gases ($\gamma = 5/3$). A micro-Macro fluid model of form (2.6)–(2.7) can be derived.

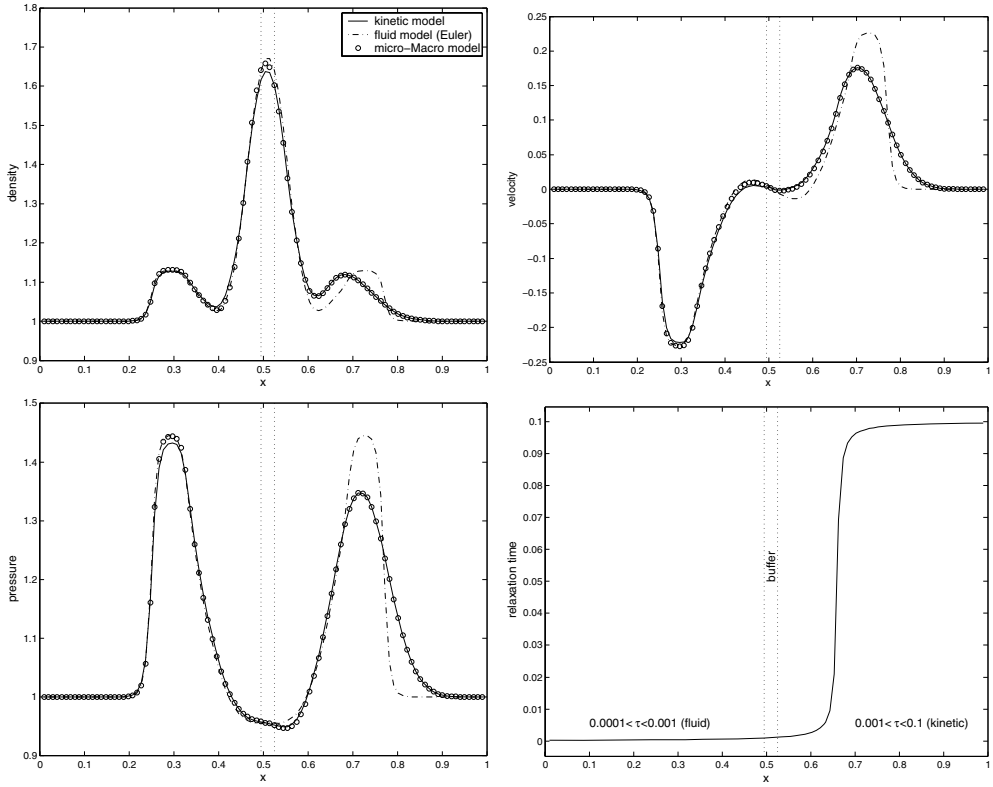

FIG. 6. *The numerical solution at* $t = 0.1103$ *of density (top left), velocity (top right), and pressure (bottom left) for the* $1D$ *BGK model* (3.14) *with a space dependent relaxation time (from* 0.0001 *to* 0.1*, plotted bottom right).*

We use the classical stationary normal shock wave problem (see [33] or [4]). The gas is initially into two uniform left and right Maxwellian states separated by a discontinuity at $x = 0$. The two states are related by the Rankine–Hugoniot relations. The steady state shows the smooth transition between upstream and downstream states. For the upstream flow, we used a density $n = 6.63 \times 10^{-6}$ kg.m^{-3}, a velocity $u = 2551$ m.s^{-1}, and a temperature $T = 293$ K. These values yield a shock Mach number of 8.

Contrary to the previous models, the present model does not explicitly contain a small parameter that could indicate where the kinetic effects should be taken into account. However, it seems clear that the flow is very close to equilibrium far away from the shock and in a highly nonequilibrium state within the shock. Actually, this can be made more precise by plotting the local Knudsen number $Kn = \frac{\text{mean free path}}{n/\partial_x n}$ obtained with a full BGK computation (see Figure 8). According to Bird [4], the upper limit on Kn at which a kinetic description must be used may be taken to be 0.2. Consequently, we define three different zones where the kinetic upscaling will be used: these zones are, respectively, defined by $Kn > 10^{-2}, 10^{-3}, 10^{-4}$. We do not use the upper limit $Kn > 0.2$ given by Bird, since it would give a very narrow zone.

For the numerical computation, we use a finite space domain $[-0.5, 0.5]$ discretized with a uniform mesh of 300 cells. The velocity domain is $[-3410, 4603]$ discretized with 40 points. This ensures that both left and right Maxwellian are well represented

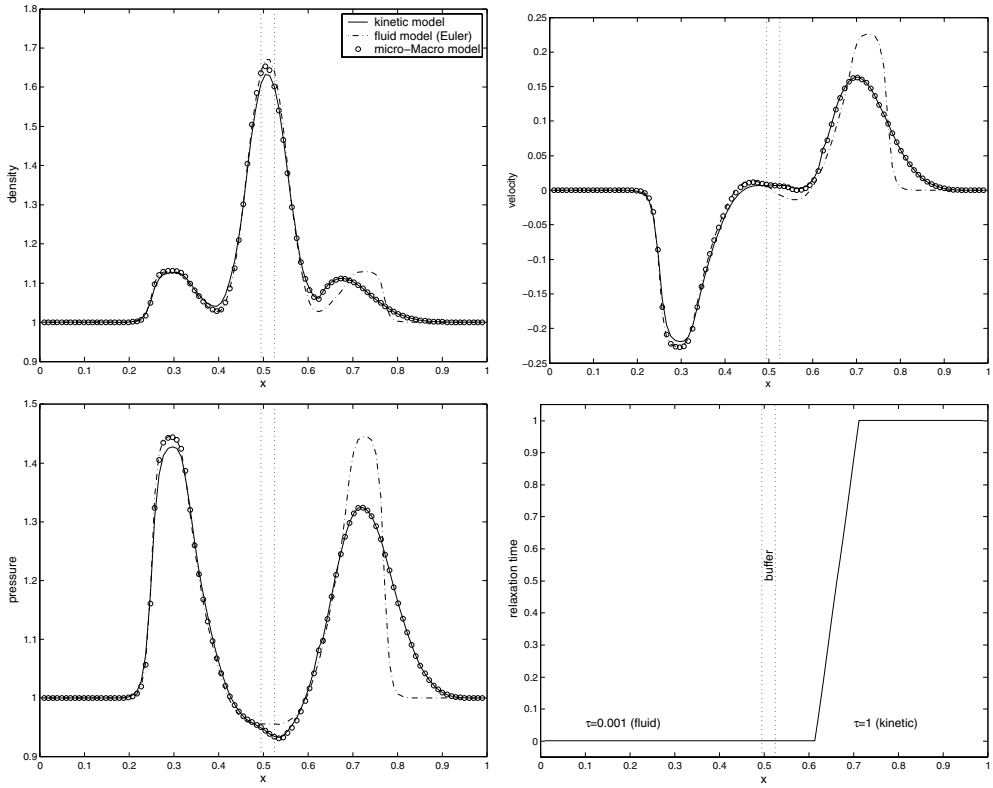

FIG. 7. *The numerical solution at* $t = 0.1103$ *of density (top left), velocity (top right), and pressure (bottom left) for the* 1*D BGK model* (3.14) *with a space dependent relaxation time (piecewise linear from* 0.001 *to* 1*, plotted bottom right).*

on the velocity grid. A second order scheme is used with the kinetic flux vector splitting of [31] for the macroscopic terms with an implicit time discretization of the collision operator. For the three tests, the kinetic zone is separated from the fluid zone by two left and a right buffer zones of length 1/30. The function h is defined with a piecewise affine function, as in previous examples (it is 1 inside the kinetic zone and 0 in the fluid zone). As usual for this test case, we use a stabilization technique to prevent the shock from moving to the right. Namely, after each time step, the solution is shifted so that the mean density point x (defined by the relation $n(x) = \frac{n_{left}+n_{right}}{2}$) is equal to 0. See [33] and the references therein for a discussion of this so-called shift-phenomenon.

In Figures 9–11, we compare the macroscopic quantities density, velocity, temperature, and heat flux obtained with a full kinetic computation to the ones obtained with our micro-Macro model, with the three different kinetic zones. We observe that for the density all the results are very close. For the other quantities, the results obtained with the two largest kinetic zones are very close to the full kinetic solution. However, the results obtained with the most narrow kinetic zone are correct only inside the shock and downstream. In the upstream part, we can clearly see a kind of discontinuity, located in the left buffer zone. This is probably due to the fact that the macroscopic model (Euler model) is used where the kinetic effects are still important, even if the local Knudsen number is lower than 10^{-2} in this zone. Note that this

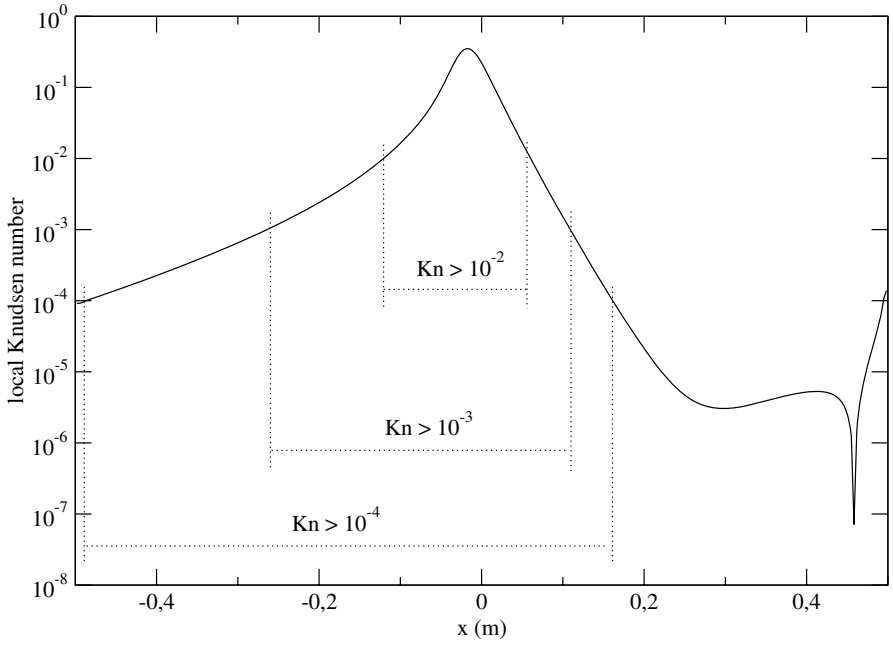

FIG. 8. *Local Knudsen number for the stationary normal shock wave (in log scale). The three zones where the kinetic upscaling will be used are represented by dotted lines.*

number is based on the density only; it is thus not surprising that it does not take into account all the nonequilibrium effects. Instead we could use much more precise criteria that exist in the literature to determine how a flow locally departs from an equilibrium state (see, for instance, [27, 32, 37]).

We also plot in Figures 12–16 the reduced distribution function $F(x, v)$ into five different points of the flow: $x = -0.1383$ (upstream), $x = -0.2217$ (left part of the shock), $x = 0$ (middle of the initial shock), $x = 0.0117$ (right part of the shock), $x = 0.0717$ (downstream). We find that all the results are very close (even if the results obtained with the most narrow zone are less accurate than the others).

This test thus shows that our micro-Macro model behaves fairly well to describe rarefied gas problems. However, we think that the macroscopic model (Euler equations) is not very well adapted for this case. Indeed, the solution given by the Euler model is simply the initial discontinuity, which is very far from the kinetic solution, in particular in the upstream flow. Instead, we could probably use a much narrower kinetic zone if the macroscopic model was Navier–Stokes equations instead of Euler equations. The derivation of such micro-Macro model is deferred to a future work.

Example 6.4. Numerical solution of the micro-Macro model for the radiative heat transfer problem.

We solve the kinetic problem (4.12)–(4.13), the asymptotic diffusion model (4.18), and the micro-Macro model (4.25)–(4.26) in the domain $[0, 1]$. We use Dirichlet boundary conditions for the temperature:

$$T(t, 0) = 1, \qquad T(t, 1) = 0,$$

and equilibrium Dirichlet boundary conditions for the radiative intensity:

$$I(t, 0, \mu) = 1, \quad \mu > 0, \qquad I(t, 1, \mu) = 0, \quad \mu < 0.$$

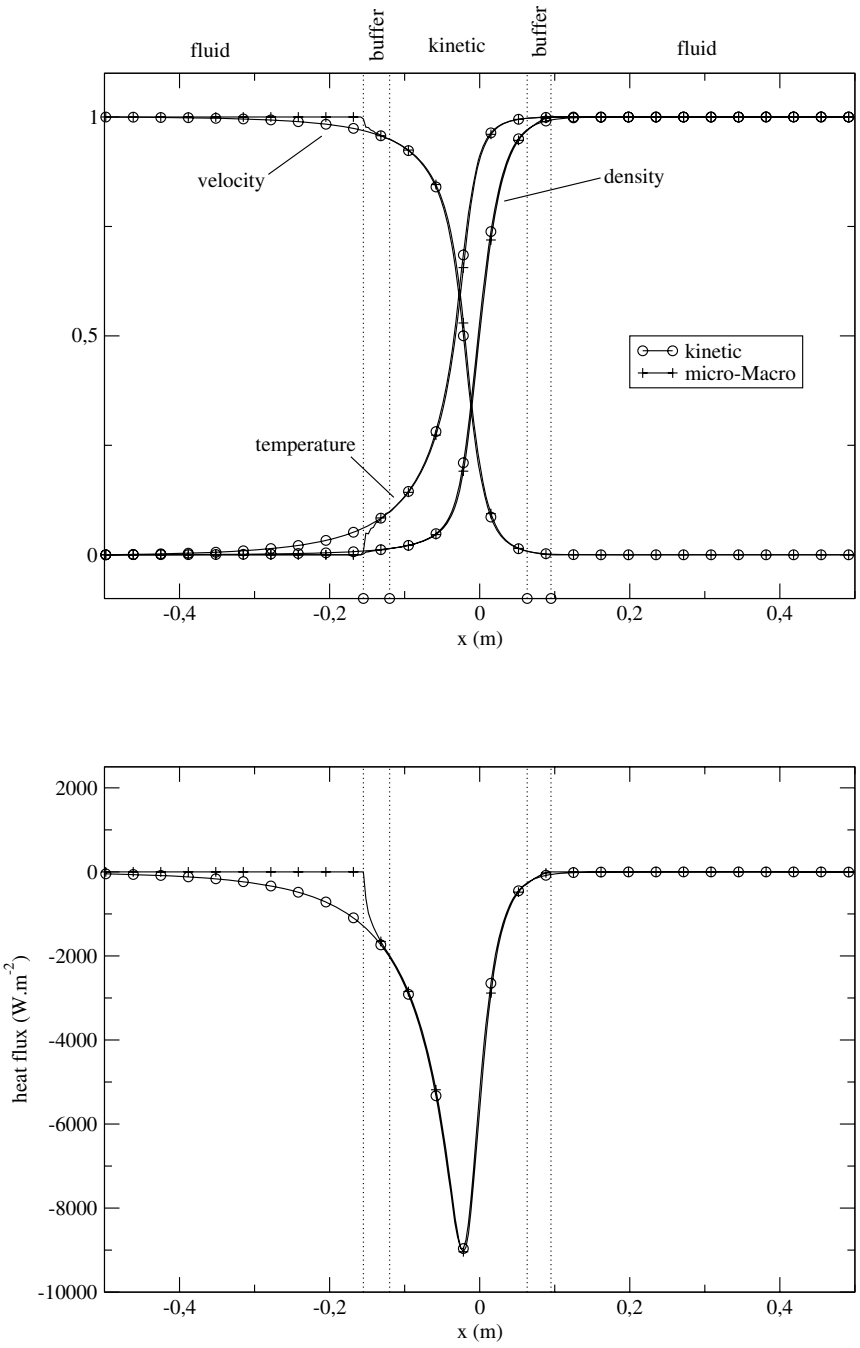

FIG. 9. *Density, velocity, and temperature (top) and heat flux (bottom) for the stationary normal shock wave. Comparison of the full kinetic BGK equation to the micro-Macro model with a kinetic zone defined by a local Knudsen number greater than* 10^{-2}.

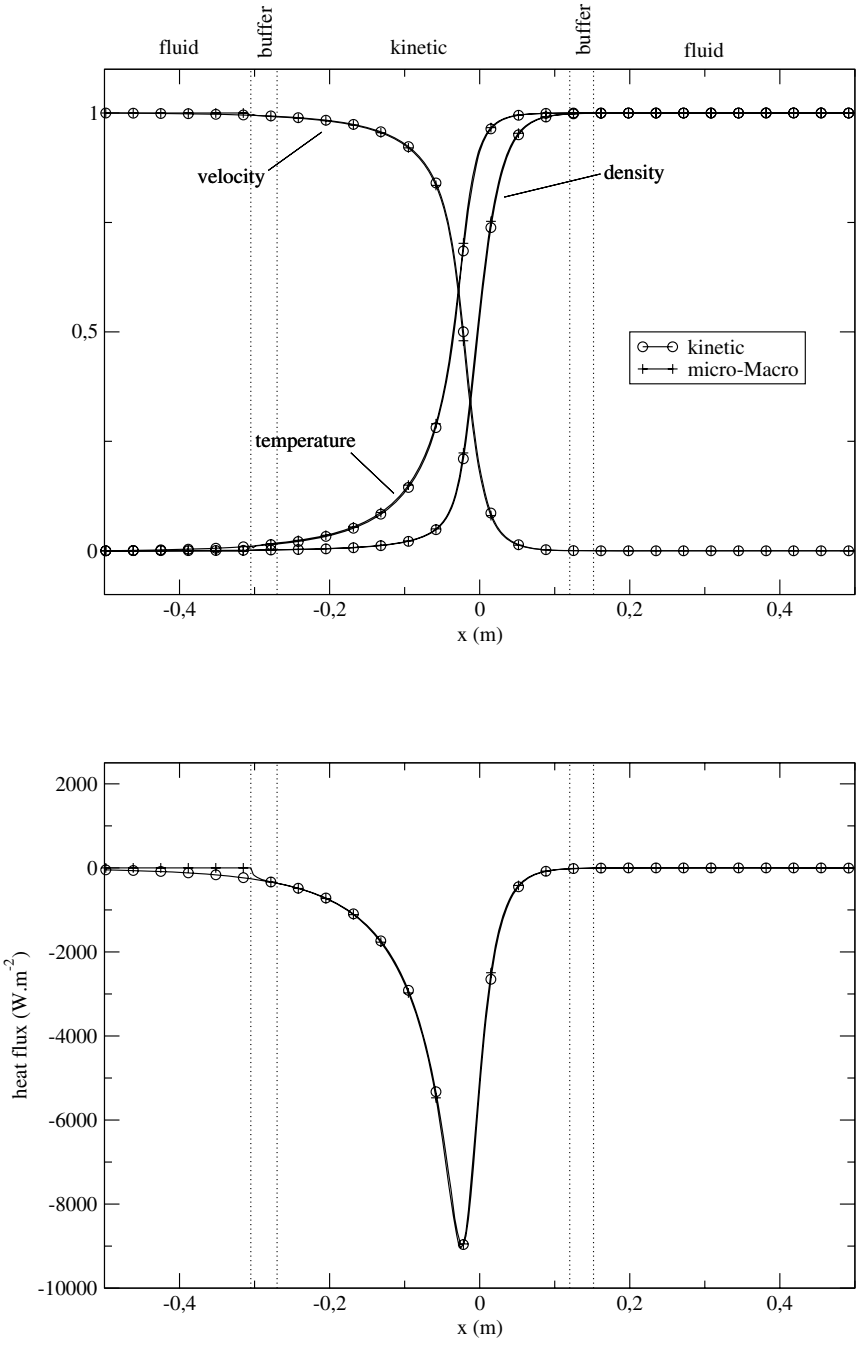

FIG. 10. *Density, velocity, and temperature (top) and heat flux (bottom) for the stationary normal shock wave. Comparison of the full kinetic BGK equation to the micro-Macro model with a kinetic zone defined by a local Knudsen number greater than* 10^{-3}.

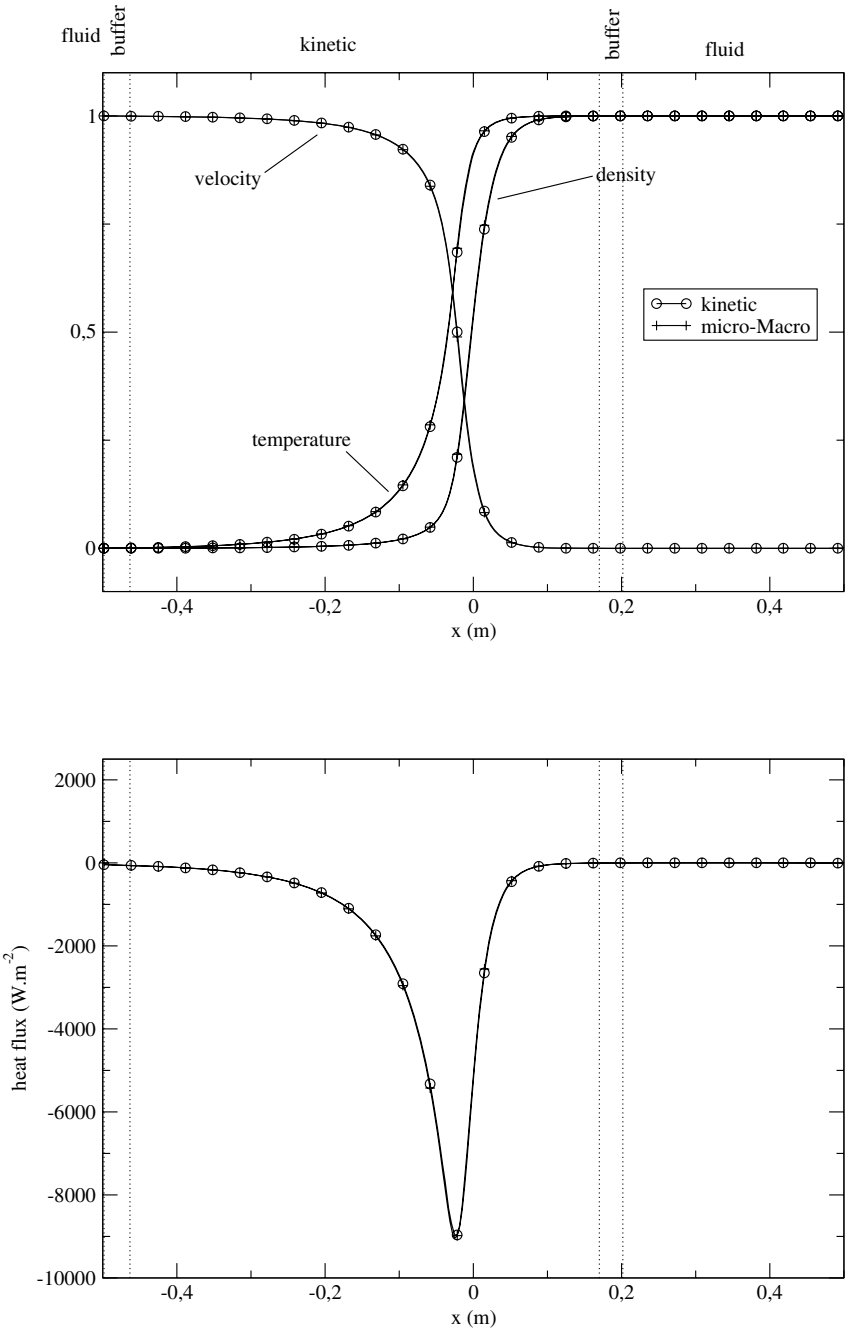

FIG. 11. *Density, velocity, and temperature (top) and heat flux (bottom) for the stationary normal shock wave. Comparison of the full kinetic BGK equation to the micro-Macro model with a kinetic zone defined by a local Knudsen number greater than* 10^{-4}.

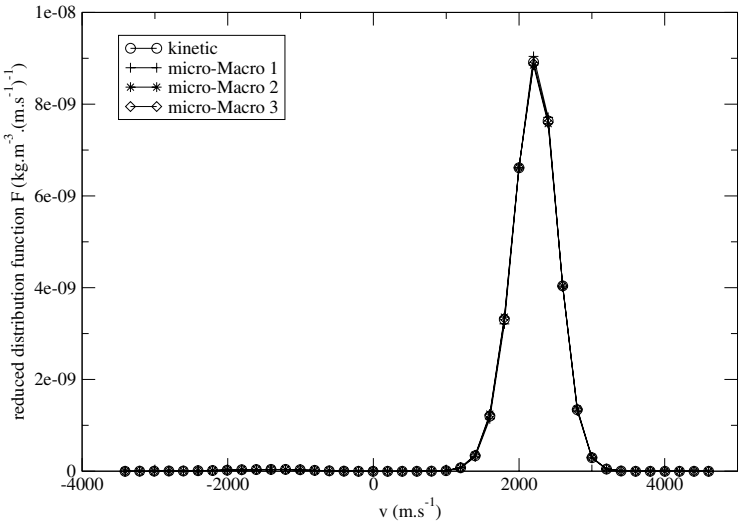

FIG. 12. *Stationary normal shock wave problem: reduced distribution function* $F(x,v)$ *at* $x = -0.1383$ *m (upstream) for BGK and micro-Macro model used with three different kinetic zones* (1: $Kn > 10^{-2}$, 2: $Kn > 10^{-2}$, 3: $Kn > 10^{-2}$).

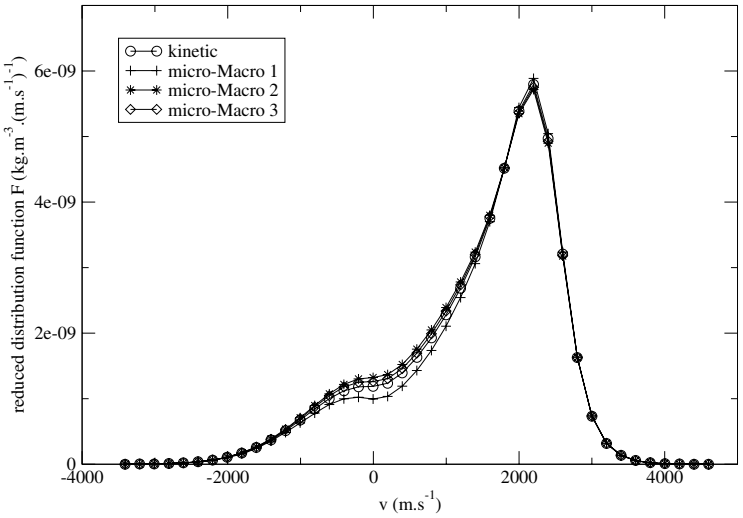

FIG. 13. *Stationary normal shock wave problem: reduced distribution function* $F(x,v)$ *at* $x = -0.0217$ *m (left part of the shock) for BGK and micro-Macro model used with three different kinetic zones* (1: $Kn > 10^{-2}$, 2: $Kn > 10^{-2}$, 3: $Kn > 10^{-2}$).

The corresponding boundary conditions for g_K are

$$g_K(t,0,\mu) = 0, \quad \mu > 0, \qquad g_K(t,1,\mu) = 0, \quad \mu < 0.$$

The initial data are $I|_{t=0} = T|_{t=0} = 0$, and thus $g_K|_{t=0} = 0$.

In this example, we take $\varepsilon = 1$, and the value of the opacity σ characterizes the nature of the regime (transport or diffusive). It is defined to be piecewise linear

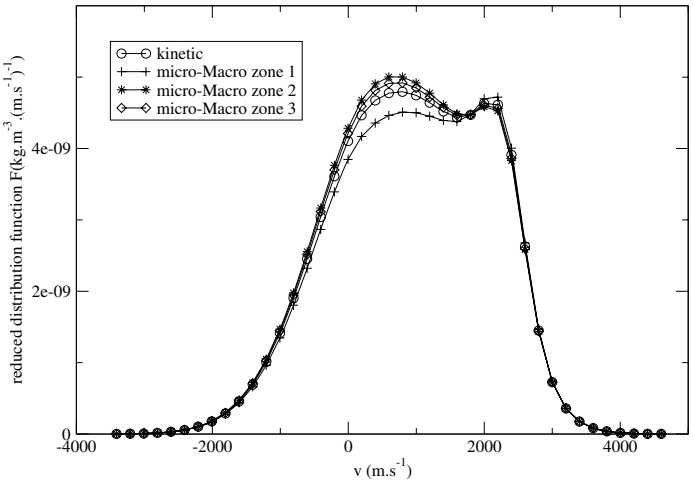

FIG. 14. *Stationary normal shock wave problem: reduced distribution function* $F(x, v)$ *at* $x =$ 0 *m (in the shock) for BGK and micro-Macro model used with three different kinetic zones* (1: $Kn > 10^{-2}$, 2: $Kn > 10^{-2}$, 3: $Kn > 10^{-2}$).

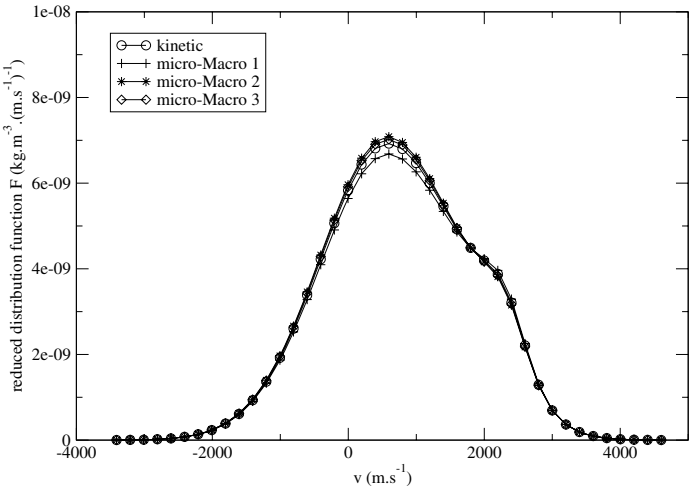

FIG. 15. *Stationary normal shock wave problem: reduced distribution function* $F(x, v)$ *at* $x =$ 0.0117 *m (right part of the shock) for BGK and micro-Macro model used with three different kinetic zones* (1: $Kn > 10^{-2}$, 2: $Kn > 10^{-2}$, 3: $Kn > 10^{-2}$).

and continuous: 1 for $x \leq 0.1$, 100 for $x \geq 0.15$, and linear between 0.1 and 0.15. Therefore we can consider that the interval $[0, 0.1]$ is purely kinetic, while $[0.15, 1]$ is purely diffusive.

The function h is also defined to be piecewise linear and continuous: 0 for $x \leq a$, 1 for $x \geq b$, and linear between a and b. We use two choices of buffer zones: $a = 0.12$, $b = 0.17$; $a = 0.16$, $b = 0.21$, respectively. Note that these buffers have the same size, while only the second one is inside the fluid zone (this was suggested by the analysis given in section 3.2).

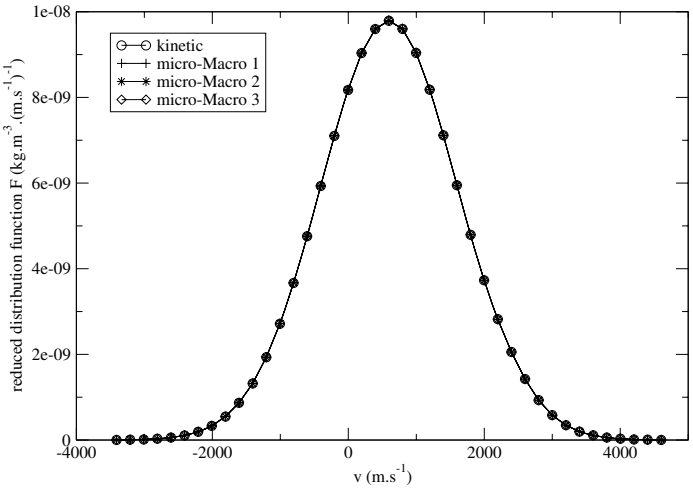

FIG. 16. *Stationary normal shock wave problem: reduced distribution function* $F(x, v)$ *at* $x = 0.0717$ *m (downstream) for BGK and micro-Macro model used with three different kinetic zones* (1: $Kn > 10^{-2}$, 2: $Kn > 10^{-2}$, 3: $Kn > 10^{-2}$).

We use 100 points for x and 20 points for μ. We compute both transient and steady states.

In the different figures, the temperature of the kinetic model is plotted with a solid line, while the temperature of the micro-Macro model is shown by the symbol "o." We also plot the temperature of the full diffusion limit with a dash-dotted line. The buffer zone is made clearly visible by two vertical dotted lines at $x = a$ and $x = b$.

For the transient state ($t = 0.0185$) we observe in Figure 17 that the micro-Macro model is very close to the kinetic solution in the whole domain. This result is remarkable, since the full diffusion model itself is completely wrong, even in the diffusive domain, whereas our micro-Macro model is nothing but the full diffusion equation in the diffusion domain. This difference is due to the fact that the diffusion model fails to capture the correct dynamics in the kinetic zone, while our micro-Macro model does not.

For the steady state (Figure 18), the conclusions are similar except that with the buffer which is not completely in the fluid zone: the results obtained with this buffer are not as accurate as with the other one. This comforts the analysis given in section 3.2.

Finally, we mention that our micro-Macro model is perfectly in agreement with the diffusion equation if both domains are diffusive (say, $\sigma = 1$ everywhere). The corresponding results are not plotted here.

7. Conclusion. In this work, we have presented a method to model kinetic problems by using a fluid approximation wherever it is possible. We have proposed a way to include a localized kinetic upscaling that corrects the fluid model wherever it is necessary. In parts of the domain where the particles are very far from an equilibrium state, our method turns to the full kinetic equation, while where equilibrium state is reached, only the fluid equations are solved. The main ingredients we have used are a splitting of the distribution function into an equilibrium leading part plus a perturbative nonequilibrium term, and the idea of buffer zones and transition functions as

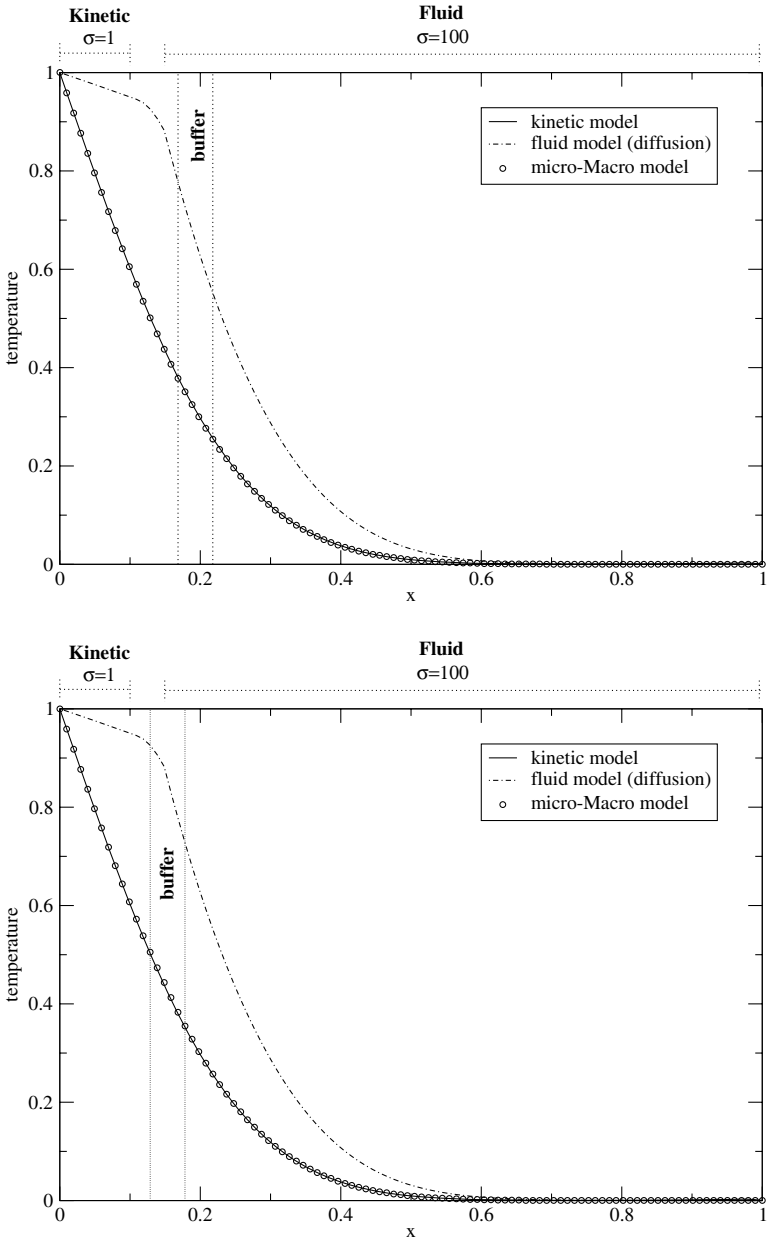

FIG. 17. *The numerical solution of the temperature for the radiative heat transfer model* (4.2) *at* $t = 0.0185$*, with a buffer inside the fluid zone (top) and a buffer partially outside the fluid zone (bottom).*

proposed in [14] and [15].

Of course, the previous numerical results are only preliminary tests. An intensive series of new tests should be done to measure the performances of our method, in particular in 2D configurations. But already, we have presented several tests in one space dimension that show our method behaves quite satisfactorily. Moreover, we

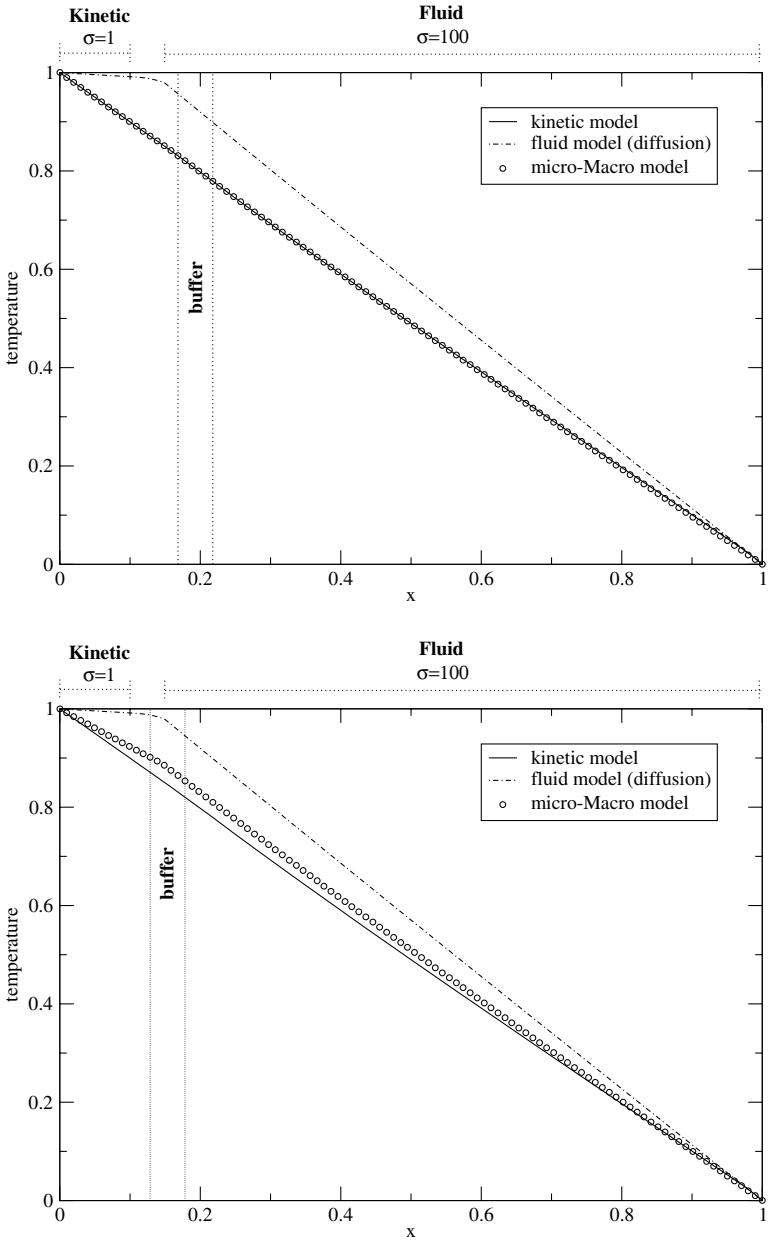

FIG. 18. *The numerical solution of the temperature for the radiative heat transfer model* (4.2) *at steady state, with a buffer inside the fluid zone (top) and a buffer partially outside the fluid zone (bottom).*

have shown that our method raises the main question addressed in [15], while it shares many similar properties. It is very easy to use and to implement, since the zones where the kinetic upscaling is taken into account are defined through a function which is evaluated once for all on the grid. For instance, several kinetic subdomains with nonconnex buffer zones can easily be used without modifying the implementation.

Moreover, its simplicity allows us to apply it to very different problems, such as rarefied gas dynamics and radiative heat transfer.

Further developments of this work could include the use of a time-dependent transition function h coupled with a physical criterion to obtain an adaptive micro-Macro model as it is done in [13]. It is also very important to build asymptotic preserving schemes for micro-Macro models that account for diffusion scale, like the radiative heat transfer model. Moreover, for the case of rarefied gas dynamics, it should be very relevant to extend our approach to a micro-Macro model whose fluid model would be the Navier–Stokes equations rather than the Euler equations. Finally, we shall also try to apply this method in other physical problems where multiscale effects are important.

REFERENCES

[1] F. F. Abraham, J. Q. Broughton, N. Bernstein, and E. Kaxiras, *Spanning the continuum to quantum length scales in a dynamic simulation of brittle fracture*, Europhys. Lett., 44 (1998), pp. 783–787.

[2] G. Bal and Y. Maday, *Coupling of transport and diffusion models in linear transport theory*, M2AN Math. Model. Numer. Anal., 36 (2002), pp. 69–86.

[3] P. L. Bathnagar, E. P. Gross, and M. Krook, *A model for collision processes in gases.* I. *Small amplitude processes in charged and neutral one-component systems*, Phys. Rev., 94 (1954), pp. 511–525.

[4] G. A. Bird, *Molecular Gas Dynamics and the Direct Simulation of Gas Flows*, Oxford Engrg. Sci. Ser. 42, Clarendon Press, Oxford University Press, New York, 1995.

[5] J.-F. Bourgat, P. Le Tallec, and M. D. Tidriri, *Coupling Boltzmann and Navier-Stokes equations by friction*, J. Comput. Phys., 127 (1996), pp. 227–245.

[6] W. Cai, M. de Koning, V. V. Bulatov, and S. Yip, *Minimizing boundary reflections in coupled-domain simulations*, Phys. Rev. Lett., 85 (2000), pp. 3213–3216.

[7] C. Cercignani, *The Boltzmann Equation and Its Applications*, Appl. Math. Sci. 67, Springer-Verlag, New York, 1988.

[8] S. Chandrasekhar, *Radiative Transfer*, Dover, New York, 1960.

[9] S. Chen, W. E, Y. Liu, and C.-W. Shu, *A Domain Decomposition Method for Kinetic-Hydrodynamic Multiscale Problems in Gas Dynamics and Device Simulations Using the Discontinuous Galerkin Method*, preprint.

[10] H. Choi and J.-G. Liu, *The reconstruction of upwind fluxes for conservation laws: Its behavior in dynamic and steady state calculations*, J. Comput. Phys., 144 (1998), pp. 237–256.

[11] N. Crouseilles, P. Degond, and M. Lemou, *A hybrid kinetic/fluid model for solving the gas dynamics Boltzmann-BGK equation*, J. Comput. Phys., 199 (2004), pp. 776–808.

[12] N. Crouseilles, P. Degond, and M. Lemou, *A hybrid kinetic-fluid model for solving the Vlasov-BGK equation*, J. Comput. Phys., 203 (2005), pp. 572–601.

[13] P. Degond, G. Dimarco, S. Jin, and L. Mieussens, *A Dynamic Transition between Kinetic and Hydrodynamic Equations*, manuscript.

[14] P. Degond and S. Jin, *A smooth transition model between kinetic and diffusion equations*, SIAM J. Numer. Anal., 42 (2005), pp. 2671–2687.

[15] P. Degond, S. Jin, and L. Mieussens, *A smooth transition model between kinetic and hydrodynamic equations*, J. Comput. Phys., 209 (2005), pp. 665–694.

[16] P. Degond and C. Schmeiser, *Kinetic boundary layers and fluid-kinetic coupling in semiconductors*, Transport Theory Statist. Phys., 28 (1999), pp. 31–55.

[17] W. E and B. Engquist, *The heterogeneous multiscale method*, Commun. Math. Sci., 1 (2003), pp. 87–132.

[18] W. E and Z. Huang, *A dynamic atomistic-continuum method for the simulation of crystalline materials*, J. Comput. Phys., 182 (2002), pp. 234–261.

[19] F. Golse, S. Jin, and C. D. Levermore, *A domain decomposition analysis for a two-scale linear transport problem*, M2AN Math. Model. Numer. Anal., 37 (2003), pp. 869–892.

[20] A. B. Huang and P. F. Hwang, *Test of statistical models for gases with and without internal energy states*, Phys. Fluids, 16 (1973), pp. 466–475.

[21] G.-S. Jiang and C.-W. Shu, *Efficient implementation of weighted ENO schemes*, J. Comput. Phys., 126 (1996), pp. 202–228.

[22] S. Jin and Z. P. Xin, *The relaxation schemes for systems of conservation laws in arbitrary*

space dimensions, Comm. Pure Appl. Math., 48 (1995), pp. 235–276.

[23] A. Klar, *Asymptotic-induced domain decomposition methods for kinetic and drift diffusion semiconductor equations*, SIAM J. Sci. Comput., 19 (1998), pp. 2032–2050.

[24] A. Klar, H. Neunzert, and J. Struckmeier, *Transition from kinetic theory to macroscopic fluid equations: A problem for domain decomposition and a source for new algorithms*, Transport Theory Statist. Phys., 29 (2000), pp. 93–106.

[25] A. Klar and C. Schmeiser, *Numerical passage from radiative heat transfer to nonlinear diffusion models*, Math. Models Methods Appl. Sci., 11 (2001), pp. 749–767.

[26] A. Klar and N. Siedow, *Boundary layers and domain decomposition for radiative heat transfer and diffusion equations: Applications to glass manufacturing process*, European J. Appl. Math., 9 (1998), pp. 351–372.

[27] C. D. Levermore, W. J. Morokoff, and B. T. Nadiga, *Moment realizability and the validity of the Navier-Stokes equations for rarefied gas dynamics*, Phys. Fluids, 10 (1998), pp. 3214–3226.

[28] X. Li and W. E, *Multiscale modeling of the dynamics of solids at finite temperature*, J. Mech. Phys. Solids, 53 (2005), pp. 1650–1685.

[29] T.-P. Liu and S.-H. Yu, *Boltzmann equation: Micro-macro decompositions and positivity of shock profiles*, Comm. Math. Phys., 246 (2004), pp. 133–179.

[30] X.-D. Liu, S. Osher, and T. Chan, *Weighted essentially non-oscillatory schemes*, J. Comput. Phys., 115 (1994), pp. 200–212.

[31] J. C. Mandal and S. M. Deshpande, *Kinetic flux vector splitting for Euler equations*, Comput. & Fluids, 23 (1994), pp. 447–478.

[32] T. Ohsawa and T. Ohwada, *Deterministic hybrid computation of rarefied gas flows*, in Proceedings of the 23rd International Symposium on Rarefied Gas Dynamics, Vol. 663, American Institute of Physics, Melville, NY, 2003, pp. 931–938.

[33] T. Ohwada, *Structure of normal shock waves: Direct numerical analysis of the Boltzmann equation for hard-sphere molecules*, Phys. Fluids A, 5 (1993), pp. 217–234.

[34] B. Perthame, *Second-order Boltzmann schemes for compressible Euler equations in one and two space dimensions*, SIAM J. Numer. Anal., 29 (1992), pp. 1–19.

[35] Y. Qiu, *Étude des équations d'Euler et de Boltzmann et de leur couplage. Application à la simulation numérique d'écoulements hypersoniques de gaz raréfiés*, Institut National de Recherche en Informatique et en Automatique (INRIA), Rocquencourt, France, 1993, Thèse, Université Paris VI, Paris, 1993.

[36] J. Schneider, *Direct coupling of fluid and kinetic equations*, Transport Theory Statist. Phys., 25 (1996), pp. 681–698.

[37] P. Le Tallec and F. Mallinger, *Coupling Boltzmann and Navier-Stokes equations by half fluxes*, J. Comput. Phys., 136 (1997), pp. 51–67.

[38] S. Tiwari, *Coupling of the Boltzmann and Euler equations with automatic domain decomposition*, J. Comput. Phys., 144 (1998), pp. 710–726.

[39] G. J. Wagner, E. G. Karpov, and W. K. Liu, *Molecular dynamics boundary conditions for regular crystal lattices*, Comput. Methods Appl. Mech. Engrg., 193 (2004), pp. 1579–1601.

[40] H. C. Yee, *A Class of High-Resolution Explicit and Implicit Shock-Capturing Methods*, Technical Report Lecture Series 1989-04, von Karman Institute for Fluid Dynamics, Rhode-Saint-Genèse, Belgium, 1989.